CHALMERS

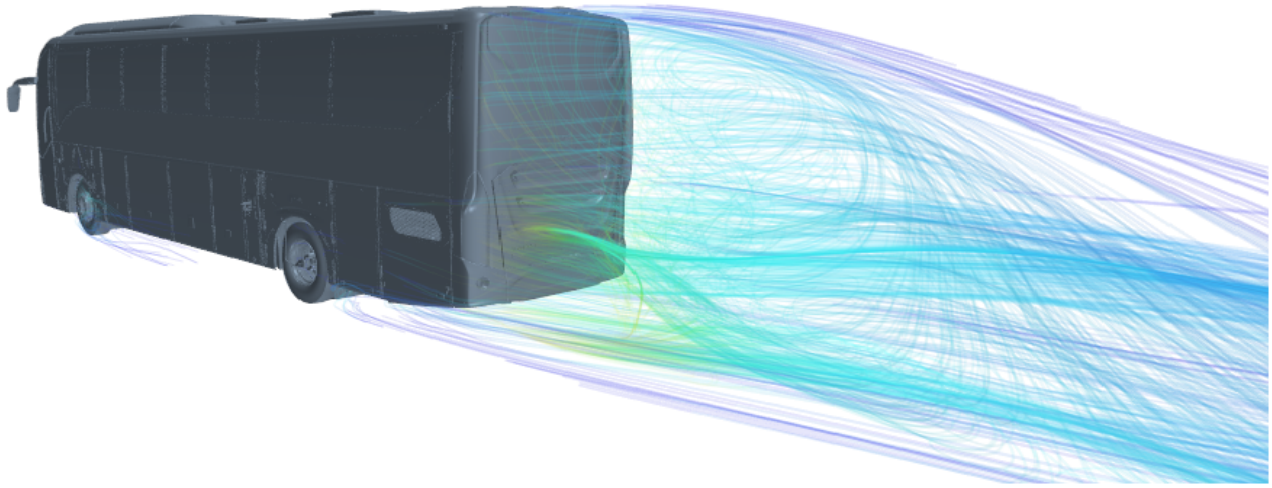

Underhood Thermal Simulation

Master's thesis in Applied Mechanics

JORACIN GERALDINI JOHN WILLIO

Department of Mechanics and Maritime Sciences
CHALMERS UNIVERSITY OF TECHNOLOGY
Göteborg, Sweden 2020

MASTER'S THESIS IN APPLIED MECHANICS

Underhood Thermal Simulation

JORACIN GERALDINI JOHN WILLIO

Department of Mechanics and Maritime Sciences
Division of Fluid Dynamics
CHALMERS UNIVERSITY OF TECHNOLOGY
Göteborg, Sweden 2020

Underhood Thermal Simulation
JORACIN GERALDINI JOHN WILLIO

Master's thesis 2020:76
Department of Mechanics and Maritime Sciences
Division of Fluid Dynamics
Chalmers University of Technology
SE-412 96 Göteborg
Sweden
Telephone: +46 (0)31-772 1000

Cover:
Temperature streamlines around the bus model

Chalmers Reproservice
Göteborg, Sweden 2020

Underhood Thermal Simulation
Master's thesis in Applied Mechanics
JORACIN GERALDINI JOHN WILLIO
Department of Mechanics and Maritime Sciences
Division of Fluid Dynamics
Chalmers University of Technology

Abstract

With an increasing necessity to control emissions and providing a sustainable transport system, it is essential to predict the cooling system performance early in the development process of the coach bus. Setting up a simulation methodology that accurately predicts the cooling system performance requires integrating cooling system performance predictions with the whole underhood thermal simulation model. The integrated simulation model is incorporated with a scope to find hot air recirculation and engine compartment backpressure, which plays a pivotal role in estimating the cooling system's performance in the coach bus.

In this work, dual-stream heat exchanger model is implemented for all three heat exchangers, namely CAC, Oil cooler, Radiator cooler. Each heat exchangers have a hot and cold interface that is provided with porous media coefficient values. The cold and hot fluid flow surpasses the respective interfaces with the specified resistance values, and thereby, heat transfer occurs. Q maps from the supplier data are used to calculate the heat exchangers' local heat transfer rate. The commercial code used to build this simulation model is STAR-CCM+.

The simulation model is tested with four different running conditions and compared with the physical test values. The pressure drop values have an excellent agreement with the supplier data from which the usage of porous coefficients is justified. The heat exchangers' power should not be a problem as they are specified through the 'Q map.' The Oil coolers, one of the heat exchangers, do not have test data, which causes deviations in CAC and radiator parameters. The lack of test data for oil coolers and radiation not being modeled causes the recirculation temperature predicted by the model to vary from test results.

Keywords: STAR-CCM+, CFD, Heat transfer,dual stream heat exchangers,GT-SUITE

Preface

This thesis project work is carried out between January 2020 - June 2020 at Volvo Bus Corporation. The project is supervised by Bastian Nebenfuhr at Volvo Bus Corporation and examined by Lars Davidson at Chalmers university. The project's objective is to develop a 3D simulation model that could be used to find the performance of cooling system before the production stage.

Acknowledgements

First of all, I would like to thank every individual involved in helping the project shape out well . A special Thanks to Bastian Nebenfuhr for providing me the opportunity and lending continuous support throughout project, amidst the Covid-19 crisis time.
I would like to thank the group manager Camilla Karlsson at Volvo buses Corporation for taking the effort to rope in all the necessary equipment's required for this project
I would also like to thank the whole virtual verification group for providing me a good environment to work and special thanks to the CFD team for the affability.
Also, I would like to thank Lars Davidson from Chalmers university for examining the thesis.
Finally, I would like to thank CD-Adapco for providing Star-CCM+ software license and BETA CAE systems for ANSA software license.

Nomenclature

CFD	-	Computational Fluid Dynamics
VBC	-	Volvo Bus Corporation
CAC	-	Charge Air Cooler
RANS	-	Reynolds Averaged Naiver Stokes
CAD	-	Computer Aided Design
LSQ	-	Least Square Gradient
IMTD	-	Inlet Manifold Temperature Difference
LAT	-	Limiting Ambient Temperature
EATS	-	Exhaust gas After Treatment System
GBX	-	Gear Box

Symbols

τ_{ij}	-	Stress tensor
ρ	-	Density
μ	-	Dynamic viscosity
ν	-	Kinematic viscosity
S_{ij}	-	Strain rate tensor
ν_t	-	Turbulent viscosity
g_i	-	Gravity
C_f	-	Skin friction
$u+$	-	Non-dimensional velocity
$y+$	-	non dimensional wall distance
u_τ	-	wall friction velocity
τ_w	-	Wall sheer stress
Re	-	Reynolds number
κ	-	Von Karman constant

Contents

1 Introduction

1.1 Background

Meeting the emission requirements is one of the primary tasks of the vehicle manufactures. Through continuous modifications over the years, engineers have achieved a compact design for the engine and cooling system. Testing these improved designs requires an exact prototype, which indeed implies a heavy toll on cost and time consumption. Replacing the testing process with the simulation model drastically simplifies the workflow and allows the engineers to scale up cooling systems' efficiency.

Though there are 3D models available for the cooling systems, some important factors could give a good estimate on the overall design, which a stand-alone cooling system model cannot predict. One such factor is hot air re-circulation. Thus, Developing a simulation model that combines the cooling system model with the underhood thermal simulation model is essential.

The 1D model generates good results on which engineers can rely on, but again it comes up with the same limitations on predicting the recirculation temperatures. Radical representation of actual process also adds up to preferring 3D over 1D.

A model of a 13L couch bus is used for the simulation.

1.2 Purpose

The simulation being 3D allows a lucid visualization and understanding of the process. This simulation model's main purpose is to cut down the cost and time required for physical testing. The simulation model allows us to test the cooling system's performance and thereby evaluate before the product production process commences. Also, the physical testing imposes greater difficulties in estimating the parameters of interest such as mass flows, pressure drops and amount of heat exchanged. Additionally, the simulation model reduces the tedious workflow involved in the physical testing process. Modeling heat exchangers as dual stream is also one of the vital aspects of this thesis.

1.3 Limitations

It is a well-known fact that the simulations models are always a simplification from the actual physics. The model itself has few limitations in terms of replicating the real-world scenarios. Coolant flowing from the engine to heat exchangers should pass through coolant jackets around the engine blocks. In the simulation model, the pipes carrying coolant were modified to be convenient for prescribing the boundary conditions. This certainly will affect heat deduction.
Simulation in 3D is more time consuming than a 1D simulation.

2 Theory

2.1 Governing Equations

The governing equations, as the name suggests, govern any fluid flow. The continuity equation (2.1), the momentum equation (2.2) , the energy equations (2.4) are those equations that governs a fluid flow..

$$\frac{\partial v_i}{\partial x_i} = 0 \tag{2.1}$$

In the above equation, v_i is the velocity and x_i denotes the spatial coordinate.

$$\rho \frac{dv_i}{dt} = -\frac{\partial P}{\partial x_i} + \frac{\partial \tau_{ji}}{\partial x_j} + \rho f_i \tag{2.2}$$

where the viscous stress tensor (τ_{ji}) and pressure (P) are derived from stress tensor (σ_{ij}). The time coordinate is denoted as 't' in the left-hand side of the equation.
The viscous stress tensor is expanded in the equation (2.3).

$$\tau_{ij} = 2\mu S_{ij} - \frac{2}{3}\mu S_{kk}\delta_i j \tag{2.3}$$

Note that the above equations are applied for incompressible laminar flows. S_{ij} refers to strain rate tensor and μ denotes the dynamic viscosity.
The energy equation is as follows.

$$\rho \frac{du}{dt} = P\frac{\partial v_i}{\partial x_i} + \Phi - \frac{\partial q_i}{\partial x_i} \tag{2.4}$$

where qi is expanded as,

$$q_i = -k\frac{\partial T}{\partial x_i} \tag{2.5}$$

and Φ is expanded as,

$$\Phi = 2\mu S_{ij}S_{ij} - \frac{2}{3}\mu S_{kk}S_{ii} \tag{2.6}$$

equation (2.5) refers to Fourier law and equation (2.6) denotes irreversible viscous heating.
Most of the practical fluid flows encounter turbulence. There is no specific definition for turbulence. It is just a random and distorted movement of fluid. For turbulent flows, the velocity is divided into fluctuating (v') and mean part ($\overline{v}$). These velocities are then time-averaged and substituted to replace the velocities in the continuity equation and momentum equations for laminar flow to give the Reynolds Averaged Navier-Stokes equation.

$$v = v' + \overline{v} \tag{2.7}$$

The time averaged continuity equation is as follows. This continuity equation is applicable only for incompressible flow where the density is constant.

$$\frac{\partial \overline{v_i}}{\partial x_i} = 0 \tag{2.8}$$

The time averaged momentum equation is as follows.

$$\rho \frac{\partial \overline{v}_i \overline{v}_j}{\partial x_j} = -\frac{\partial \overline{p}}{\partial x_i} + \mu \frac{\partial^2 \overline{v}_i}{\partial x_j \partial x_j} - \rho \frac{\partial \overline{v_i' v_j'}}{\partial x_j} \tag{2.9}$$

In the above equation ρ stands for density and μ stands for dynamic viscosity. The first term on the right hand side is pressure gradient term. The second term in the right side refers to viscous diffusion terms. The last term on the right hand side in the above equation is called Reynolds stress term. The above equation is not closure with unknowns in Reynolds stress. The Reynolds stress in terms of averaged quantities is modeled by eddy viscosity model approach to make the governing equations closure. To express the Reynolds stress in terms of averaged quantities the eddy viscosity makes use of turbulent viscosity. This approach is commonly called as Boussinesq assumption.

$$\overline{v_i' v_j'} = -2\nu_t \overline{s_{ij}} + \frac{2}{3}\delta_{ij}k \tag{2.10}$$

$\overline{s_{ij}}$ is called strain rate tensor and k refers to turbulent kinetic energy. The turbulent viscosity ν_t is computed by two equation model consisting of kinetic energy and dissipation rate. This is the reason the model is being called as K-Epsilon model. K-Epsilon model provides reasonably accuracy for industrial flows related to heat transfer and re- circulations. Also K-Epsilon model being computationally efficient allows us to prefer it over other models.

$$\nu_t = c_\mu \frac{k^2}{\epsilon} \tag{2.11}$$

In the above equations k(kinetic energy) and ϵ(dissipation) are modelled. C_μ is a constant value. This is called standard K-Epsilon model. This simulation Realizable K-Epsilon model proposed by [Shi+95] is preferred over standard K-Epsilon model for its accuracy. There are two main constrains governing the realizable models. They are, normal stresses cannot go negative and correlation coefficient for shear stress should not be greater than unity [Dav15].

$$\overline{v_i'}^2 \geq 0 \tag{2.12}$$

$$\frac{\overline{v_i' v_j'}}{\sqrt{(\overline{v_i'}^2\ \overline{v_j'}^2)}} \leq 1 \tag{2.13}$$

Also [Dav15] shows finding invariants and replacing normal stress with largest possible eigen values which eventually satisfies the above realizablity conditions.

$$\nu_t \leq \frac{2}{3\lambda_1} = \frac{k}{3} \tag{2.14}$$

In simple words, the difference between the standard model and the realizability model is that the standard model uses a constant C_μ. In reality, C_μ varies with the flow. The realizable model overcomes this by calculating C_μ that varies with the flow. In this way, the model predicts a better dissipation rate compared to standard models. The k equation remains the same as in the standard model. The model incorporates a new transport equation for dissipation rate, and damping function f_μ both expressed in terms of mean flow quantities. The damping coefficient of f_μ allows us to calculate C_μ.

$$\frac{\partial k}{\partial t} + \overline{v_j}\frac{\partial k}{\partial x_j} = \nu_t \left(\frac{\partial \overline{v_i}}{\partial x_j} + \frac{\partial \overline{v_j}}{\partial x_i} \right) \frac{\partial \overline{v_j}}{\partial x_i} + g_i \beta \frac{\nu_t}{\sigma_\theta} \frac{\partial \overline{\theta}}{\partial x_i} - \epsilon + \frac{\partial}{\partial x_j} \left((\nu + \frac{\nu_t}{\sigma_k}) \frac{\partial k}{\partial x_j} \right) \tag{2.15}$$

$$\frac{\partial \epsilon}{\partial t} + \overline{v_j}\frac{\partial \epsilon}{\partial x_j} = \frac{\partial}{\partial x_j} \left(\frac{\nu_t}{\sigma_\epsilon} \frac{\partial \epsilon}{\partial x_j} \right) + C_1 \overline{S_{ij}} \epsilon - C_2 \frac{\epsilon^2}{k + \sqrt{\nu\epsilon}} \tag{2.16}$$

$\overline{S_{ij}}$ refers to strain rate tensor. C_1, C_2, σ_e are constants. Further readings regarding the derivation and coefficients of this new transport equation can be found at [Shi+95]. Two-Layer Realizable k-epsilon is a combination of the Realizable K-Epsilon model and a two-layer approach. The two-layer approach developed by [ROD] is nothing but a type of wall treatment used for capturing near-wall phenomena. More details about this wall treatment are discussed below.

2.1.1 Wall treatment

The type of wall treatment to be used is decided upon a non-dimensional wall distance y^+. It is good to determine the type of wall treatment to be used early in the pre-processing stage. The below equations allow us to calculate the distance between the wall and the first cell center.

$$y^+ = \frac{y u_\tau}{\nu} \tag{2.17}$$

where y is the absolute wall distance, u_τ is the wall friction velocity and ν is the kinematic velocity. From the above equation the desired y^+ values is assumed and the equation is solved for y.

Low y^+ wall treatment

For $y^+ < 1$, low y^+ wall treatment is used. The usage of low y^+ means that the first cell's center is placed in a viscous sublayer. This requires the mesh to be sufficiently fine near the walls. Thus the low y^+ wall treatment is not computationally efficient. Viscous effects dominate the viscous sublayer.

$$u^+ = y^+ \tag{2.18}$$

High y^+ wall treatment

For $y^+ > 30$, high y^+ wall treatment is used. The high y^+ wall treatment uses wall functions to resolve the near-wall phenomenon instead of being extremely finer. The center of the first cell is placed in the log-law region.

$$u+ = \frac{1}{\kappa} ln(y^+) + B \tag{2.19}$$

B is the integeration, κ is the Von Karman constant.

Two layer All y^+ wall treatment

The Two-layer All y^+ wall treatment is a hybrid approach. It combines low and high y^+ wall treatment methods. This approach can account for both coarser and finer mesh near the walls. Another highlight of this approach is that it also accounts for mesh falling in an intermediate region called buffer region. The two-layer all y^+ treatment is exactly the same as all y^+ wall treatment except a single aspect. The two-layer formulations of K-Epsilon equations impose a new transport equation for ϵ. The two-layer all y^+ wall treatment is specially used to suit these formulations.

2.2 Heat transfer

2.2.1 Convection

Convection is a process in which the exchange of heat and energy takes by the fluid's motion. The bulk transport (advection) of the fluid and random movement of molecules, which is technically called diffusion/conduction, is responsible for convective heat transfer. In heat transfers from or to the solids, conduction governs the heat transfer near the walls where the velocity is very low. Bulk movement of fluid controls the heat transfer away from the wall.

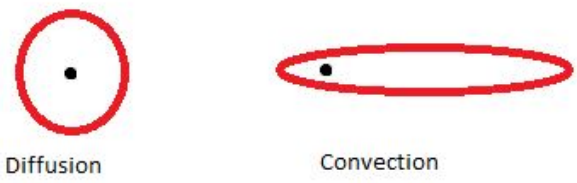

Figure 2.1: Illustration of convection and diffusion

The black color dot represents a physical quantity, and the red color shape indicates how the quantity spreads. Newton's law of cooling governs The heat convection on the surface.

$$q''_s = h(T_s - T_{ref}) \tag{2.20}$$

where h is the local convective heat transfer coefficient, q''_s is the local surface heat flux, T_s is the temperature of the surface and T_{ref} temperature of the fluid.
There are two types of convection namely natural and forced convection.

Natural Convection

Natural convection occurs due to temperature differences. Fluids with high temperatures have a lower density, and low fluids with low temperatures have high density. By nature, the high dense fluid is forced to stay below less dense fluid due to gravity. Natural convection in turbulent flow leads to a phenomenon called stratification.

Forced convection

Convection is said to be forced if external forces govern the movement of the fluids. For example, using a hydraulic pump increases the mass flow of fluid and increases the heat transfer rate.

2.2.2 Conduction

In conduction, the heat and energy transfer occurs due to interaction between molecules. The energy is transferred from higher temperature to lower temperature. Fourier law is used to calculate the temperature field. Conduction occurs in all three medium(solid, liquid, gas). The conduction is usually very intense in solid due to closely packed molecules. The heating of the iron rod at one end propagates the heat throughout the rod, is a classic example oh heat conduction.

$$q'' = -k\Delta T \tag{2.21}$$

where q'' is the heat flux , ΔT is the temperature gradient and k is thermal conductivity.

2.2.3 Radiation

Radiation is a phenomenon that does not require any medium to transfer heat. The radiation can even occur in a vacuum. The movement of charged electrons and protons causes electromagnetic waves, which is the main radiation source. Modeling radiation in this work requires heat transfer coefficient data of the different materials used in the vehicle. The radiation occurs after when the surface is exposed to a certain amount oh heat flux. Stefan-Boltzmannlaw gives the maximum amount of flux a surface can hold before it starts emitting.

$$q_b''b = \sigma T_s^4 \tag{2.22}$$

where $q_s''b$ local surface heat flux, σT_s^4 Stefan-Boltzmann constant.

2.3 Cooling system

There are three heat exchangers used for this couch bus cooling system. They are Radiator, Charge air cooler (CAC), Oil cooler. The heat exchanger used for this simulation model is of dual steam heat exchanger type. Hydraulic operated fans are used to pull in higher mass flow of air passing through the heat exchangers. The fan is placed behind the heat exchangers. The geometry of the heat exchangers used determines the overall performance of the cooling system.

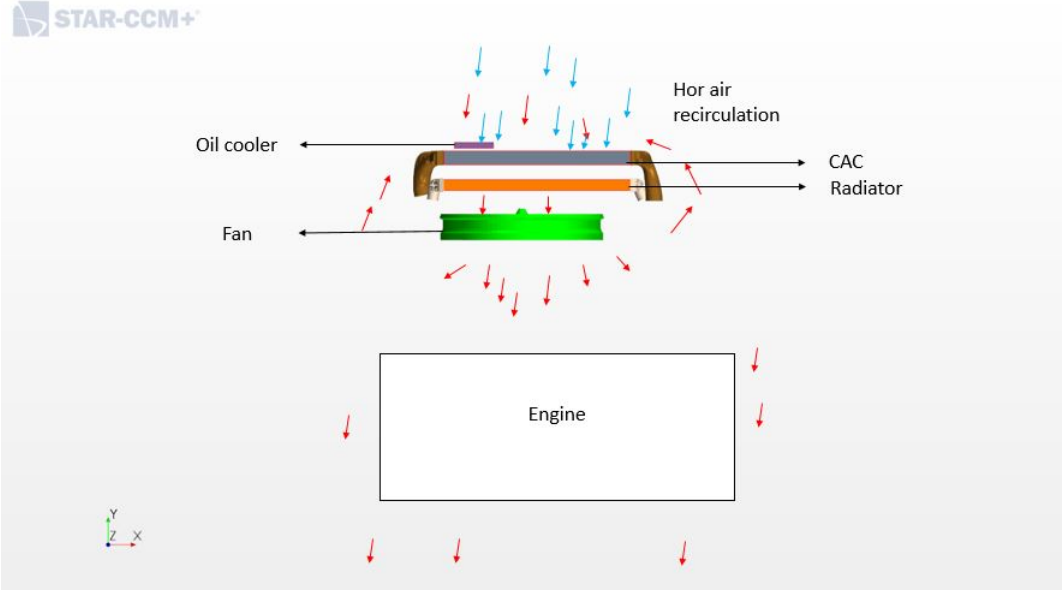

Figure 2.2: Cooling system design and Hot air recirculation

2.3.1 Dual stream heat exchangers

To understand the main advantage of dual-stream heat exchangers, it is important to get the principle idea of how the single-stream heat exchangers work. In a single stream heat exchanger, only one of the streams is modeled and the other is assumed to give a constant temperature. A common practice is that, for the heat exchangers used in automobiles, only the external side is modeled and the internal side is kept constant.

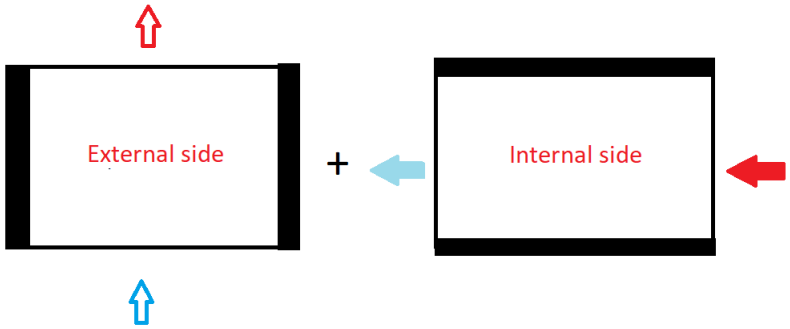

Figure 2.3: Illustration of dual-stream heat exchanger

In a dual-stream heat exchanger, both the external and internal sides are modeled. A dual-stream heat exchanger needs to have heat rejection data against both air mass flow and coolant mass flow. Q map is widely used to specify the Q value necessary for the simulation.

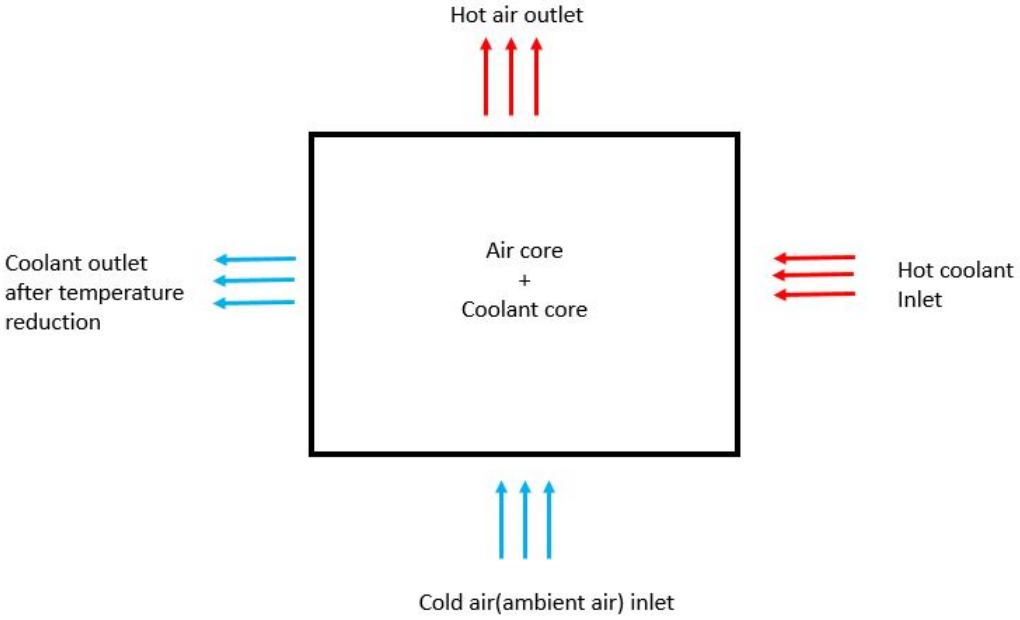

Figure 2.4: Illustration of dual stream heat exchanger

The dual-stream heat exchangers sources are added into the energy equation through equation (2.23). In the equation (2.23), the src_i is the source term in the energy equation for the cold stream and the sink term in the energy equation for the hot stream.

$$src_i = UAL_i((\frac{T_i^{hot} - T_i^{cold})V_i}{\frac{1}{NC}\sum_{i=0}^{NC} V_j}) \tag{2.23}$$

UAL_i is the local heat transfer rate, T_i^{hot} is the temperature of the hot stream in cell 'i' and T_i^{cold} is the temperature of the cold stream in cell 'i' , NC is the total number of cells in the heat exchanger region, and V_i is the volume of the cell.

$$UAL_i = \frac{\Gamma}{\Delta T_{net}} \tag{2.24}$$

ΔT_{net} is the volume averaged temperature difference between hot and cold stream in the heat exchanger region.

$$\Gamma = \frac{Q(T_{in}^{hot} - T_{in}^{cold})}{T_{user}^{hot} - T_{user}^{cold}} \tag{2.25}$$

where 'Q map' supplies the values for Q. The values in the denominator are user specified values while defining the Q map and the values in numerator are massflow averaged temperature which Star-CCM+ calculates.

2.3.2 Radiator

The engine is the most complicated part of an automotive. Numerous parts are placed close to each other in an engine. The combustion process inside the combustion chambers produces a very high temperature. This high temperature is transferred to other parts of the engine via conduction. Excessive heat should be removed in the engine components to cut down the detonation and knocking effects. It is worth mentioning that the detonation and knocking effects are the main source of increasing contaminants. The cooling is done through cooling jackets drilled around the engine block. The coolant is allowed to flow through these jackets and the, therefore, engine is cooled. In the process of cooling the engine, the coolant acquires the heat and attains a higher temperature. The hot coolant is sent to the radiator for cooling. The hot coolant is sent to the radiator, where it interacts with the ambient air (cold fluid). The coolant's temperature is lowered and it is sent back to the engine and the process repeats in a cycle.

2.3.3 CAC

The turbochargers are used to increase engine efficiency by inducing an additional volume of air. The turbocharger has a turbine and a compressor. The turbine is torqued by exhaust gas. The compressor attached to the shaft of the turbine rotates to breathe in more air. Due to compression, the air attains extremely high temperature and low density. In a motive to increase the volumetric efficiency and thereby improving the output of the engine, the compressed air is sent to a heat exchanger called Charge Air Cooler(CAC). In the CAC, the interaction between hot compressed CAC air and ambient air takes place. In this process, the hot CAC hot air is drastically cooled down and sent to the intake valve in the combustion chamber. The cooling of charge air is achieved through isochoric cooling.

2.3.4 Oil coolers

The oil coolers are used to cool down oil used in the hydraulic component. The oil used in hydraulic components gets heated up due to friction. The excessive heat in the oil causes wears and tear on the hydraulic equipment. To prevent this, the oil must be cooled upon reaching a higher temperature. Oil coolers, one of the heat exchangers used in the cooling system, is designated to do this work. The hot oil is transferred to oil coolers, where it will interact with ambient air. The oil gets cooled down and once again sent back to hydraulic components to remove the heat and the process iterates.

2.3.5 LAT

The Limiting ambient air temperature is an essential factor that needs to be checked while designing a cooling system. LAT is the maximum ambient temperature at which an engine can be operated without any malfunctions. Lower the LAT higher is the chance of engine overheating during its operation at higher temperature ambient air conditions. When LAT is higher, the temperature difference between coolant entering and exiting the radiator becomes low, which eventually imposes a higher volume of external air and increases power consumption [Bah+18].

$$LAT = (T_{max} - T_{Internal,RAD}^{In}) + T_{ambient} \tag{2.26}$$

Ambient temperature is represented by $T_{ambient}$,T_{max} refers to maximum allowed coolant temperature and $T_{Internal,RAD}^{In}$ refers to radiator coolant inlet temperature.

2.3.6 IMTD

IMTD stands for inlet manifold temperature difference. The engine inlet manifold receives air from two primary sources, as suggested above. Even after cooling, the compressed air will have a higher temperature and lower density than ambient air. This difference in air temperature on the inlet manifold affects the combustion process and thereby causing an increase in pollutants. This is the reason why it is important to have optimum value for IMTD.

$$IMTD = T^{out}_{Internal,CAC} - T_{ambient} \tag{2.27}$$

$T^{out}_{Internal} : CAC$ stands for Charge air outlet temperature.

2.3.7 Recirculation

The recirculation is an undesirable and yet unavoidable feature happening in the underhood of most of the vehicles. The complex design of the underhood system is one of the main underlying factors for the recirculation phenomenon. The recirculation has quite an impact on the cooling system. Recirculation tends to increase the coolant and charge air temperature delivered to the engine, which causes a rise in engine temperature. To maintain an optimum temperature, more external mass flow is needed. This requirement needs the fan to operate at full load, which imposes a heavy toll on electricity consumption, thereby increasing fuel consumption.

$$T_{re} = T^{In}_{External} - T_{ambient} \tag{2.28}$$

$T^{In}_{External}$ refers to temperature in the external side of the respective heat exchanger. T_{re} refers to recirculation temperature.

3 Methodology

3.1 Workflow

This section explains how the simulation model is structured and various techniques involved in setting it up.The whole of the coach bus faces ambient air. The external sides of cores in all the heat exchangers faces the ambient air as well. The internal side of the CAC faces compressed Compressed charge air from the turbo compressor.The internal side of the radiator faces hot coolant leaving after cooling the engine. Likewise, the internal side of the oil cooler faces hot hydraulic oil. The surface wrapping, meshing, and other set-ups in simulations are done, keeping this in mind.

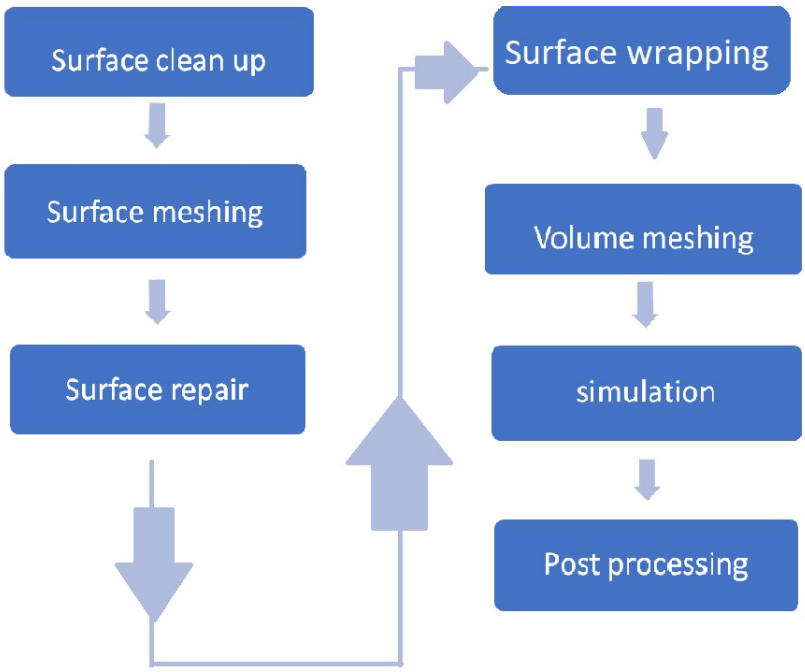

Figure 3.1: Work flow in this thesis project

The workflow in star-CCM+ is as follows. To begin with, a basic surface clean up is done in ANSA to improve the CAD. The surface meshing is done using ANSA. Once the surface meshing is done, the file is imported to Star-CCM+. In Star-CCM+, the surface repair feature is used to close holes and to imprint parts as per the need. Then the surface wrapping is done, followed by volume meshing, which is explained in the upcoming sections. Once the pre-processing stage is done, the simulation is set up, and the results are post-processed.

3.2 Terminologies

Usage of a dual-stream heat exchanger means there could be many terminologies that should be dealt with for a clear understanding of process and results. This section aims to make the readers familiar with those terminologies.

The external side and internal side forms a heat exchanger fig 2.3. The external side refers to the ambient air/cold stream side and the internal side refers to the coolant/hot stream side. In Star-CCM+ these two are different regions and different continua combined via heat exchanger interface. A detailed discussion about the interfaces is presented later in the chapter.

Symbol	Abbreviation
$\dot{m}^{In}_{External,CAC}$	Ambient air mass flow on external side CAC inlet
$\dot{m}^{Out}_{External,CAC}$	Ambient air mass flow on external side CAC outlet
$P^{In}_{External,CAC}$	Ambient air pressure at external side CAC inlet
$P^{Out}_{External,CAC}$	Ambient air pressure at external side CAC outlet
$T^{In}_{External,CAC}$	Ambient air temperature at external side CAC inlet
$T^{Out}_{External,CAC}$	Ambient air temperature at external side CAC outlet

Table 3.1: CAC external side's parameters

Symbol	Abbreviation
$\dot{m}^{In}_{Internal,CAC}$	Charge air mass flow on internal side CAC inlet
$\dot{m}^{Out}_{Internal,CAC}$	Charge air mass flow on internal side CAC outlet
$P^{In}_{Internal,CAC}$	Charge air air pressure at internal side CAC inlet
$P^{Out}_{Internal,CAC}$	Charge air air pressure at internal side CAC outlet
$T^{In}_{Internal,CAC}$	Charge air air temperature at internal side CAC inlet
$T^{Out}_{Internal,CAC}$	Charge air temperature at internal side CAC outlet

Table 3.2: CAC internal side's parameters

The tables above show the internal and external side parameters for the CAC heat exchanger. The abbreviations are similar for radiators and oil coolers.

3.3 Surface wrap

The surface meshed geometry from ANSA is imported to StarCCM+.The surface wrapper is one of the powerful tools in starCCM.The surface wrapper's purpose is to avoid gaps and intersection of surfaces that are not desired in CAD used for simulation. The surfaces which do not affect the simulation is also eliminated through the surface wrapping. The Radiator cooling package is considered to illustrate the surface wrapper. One utmost importance of surface wrapping is that it enables us to provide a contact in prevention between the parts.

3.3.1 Surface wrap methods

Figure 3.2: Largest internal volume method

The internal volume and seed point methods are used for surface wrapping in order to determine the volume of interest. The parts that are facing ambient fluid is wrapped by the internal volume method. The seed points are used when the internal flow is of importance. For example, seed points are positioned inside the heat pipes carrying coolant and charge air to wrap it.

3.3.2 Features

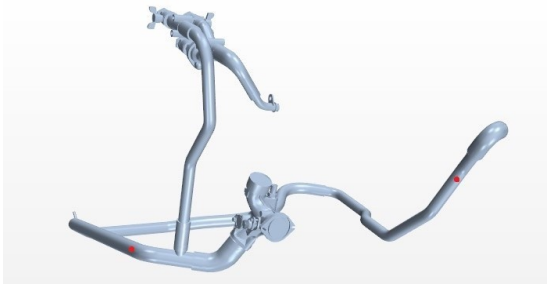

Figure 3.3: Actual geometry

Figure 3.4: Warped geometry

The above figures underline an essential feature associated with surface wrapping. The simulation model is simplified to neglect the overflows of coolant in pipes so that flow occurs only through the main pipeline in fig 3.4 and not through branches arising from it, as seen in fig 3.3. So it is good to neglect those parts for the simulation. This is achieved through wrapping via seed points placed inside the main pipeline.

3.3.3 Deviation distance

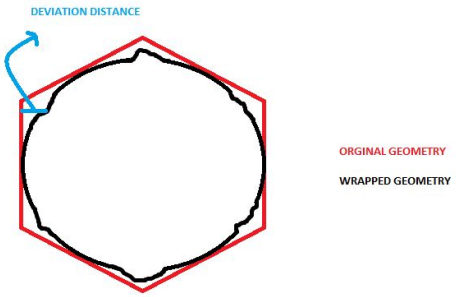

Figure 3.5: 2D illustration of surface deviation.

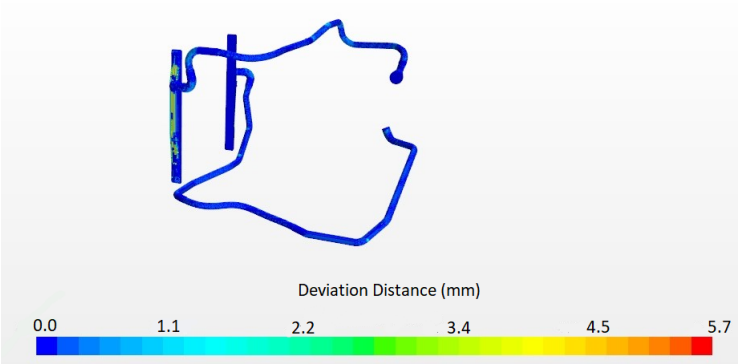

Figure 3.6: Curvature deviation in Radiator

The accuracy of surface wrapping is verified by means of curvature deviation distance. The curvature deviation distance dramatically helps achieve a better-wrapped part that resembles the actual geometry as close as

possible. The fig 3.6 gives information about how much the curvature has deviated from the actual geometry. Prescribing appropriate minimum surface size and target surface size in custom controls for those surfaces which are extremely deviated aids in increasing accuracy.

3.4 Mesh

Meshing is one of the vital aspects that determines the accuracy of any CFD simulation. Several factors need to be taken care of while meshing complex geometries. The meshing strategies vary from one part to another. It is essential to see the quality of the mesh used. Aspect ratio, skewness, mesh density, and volume ratio are factors to be considered while checking the mesh quality. A mesh quality report generated by Star-CCM+ gives a good overview of mesh quality.

3.4.1 Types of meshers

Trimmed cell mesher

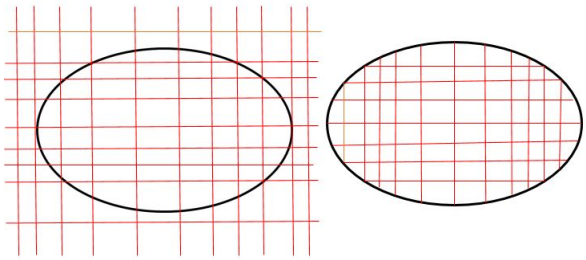

Figure 3.7: Trimmed cell mesher

The trimmed cell mesher is the most efficient when it boils down to meshing all simple and complex geometries. Trimmed cell meshers makes use of hexahedral elements predominantly. The trimmed cell mesher workflow involves generating a template mesh with user-defined target surface size around the geometry and later trimming down according to the input surface to form a core mesh. The volume mesh refinements in a trimmed cell mesher depend on local refinements and controls provided to template mesh.

Polyhedral mesher

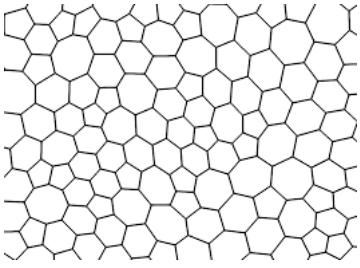

Figure 3.8: polyhedral mesh elements

The polyhedral mesher uses polyhedral elements to form the core mesh. The polyhedral mesh is generated as follows. A tetrahedral mesh is generated as an initial step. The centers of tetrahedral elements and boundary midpoints are marked and thus, the polyhedral mesh is generated starting from the outer boundary. The polyhedral mesh yields a better-resolved gradient in flow fields compared to other meshes, thereby increasing accuracy. On average, the polyhedral mesh has 12 faces due to which it has a large number of neighboring cells.

This leads to a more accurate solution than tetrahedral meshers with almost five times a lesser number of cells. Another significant advantage is that polyhedral mesh is good at predicting re-circulations.

3.4.2 Description

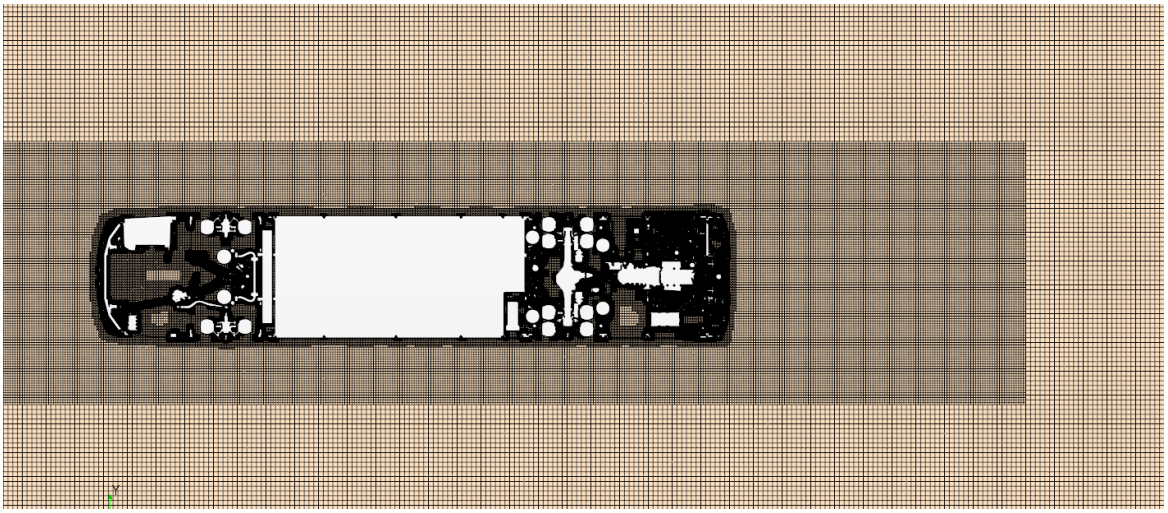

Figure 3.9: Mesh

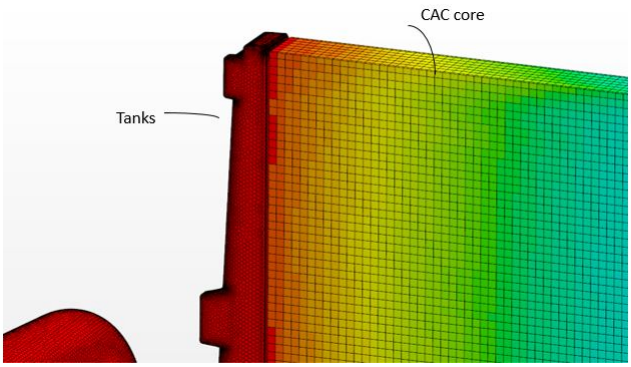

Figure 3.10: Equidistant mesh for CAC internal side

Target surface size	100%
Minimum surface size	100%
Surface growth rate	1.3
Volume growth rate	Very slow
Maximum cell size	100%

Table 3.3: Mesh settings for heat exchangers

Both the external and internal sides of a heat exchangers have been meshed with an equidistant mesh with an equal number of cells. The base size for each heat exchanger differs according to the the geometry. This is a vital aspect that determines the accuracy of the local heat transfer rate UAL_i computed. As an example, fig (3.10) shows an equidistant mesh on the CAC internal side. The trimmed cell mesher is used to mesh the heat exchangers' external and internal sides.

Base size	10 mm
Target surface size	100%
Minimum surface size	10%
Surface growth rate	1.3
Number of prism layers in interfaces	1
Number of prism layer in fan balde	12

Table 3.4: Mesh settings for fan

Base size	5 mm
Target surface size	100%
Minimum surface size	5%
Number of prism layers in interfaces	1
Number of prism layers in inlet an outlet	0
Number of prism layers in tanks and pipes	9

Table 3.5: Mesh settings for CAC tanks and pipes

Base size	10 mm
Target surface size	100%
Minimum surface size	10%
Surface growth rate	1.3
Number of prism layers in interfaces	1
Number of prism layers in inlet and outlets	0
Number of prism layers in Pipes	3
Number of prism layers in Tanks	12

Table 3.6: Mesh settings for radiator tanks and pipes

Base size	5 mm
Target surface size	100%
Minimum surface size	10%
Surface growth rate	1.3
Number of prism layers in interfaces	1
Number of prism layers in inlet an outlet	0
Number of prism layers in tanks	10
Number of prism layers in pipes	9

Table 3.7: Mesh settings for oil cooler tanks and pipes

The parts where internal flow occurs are meshed using polyhedral mesh. To be precise, the pipes, fan, coolant tanks, and charge air tanks are the parts meshed with polyhedral mesh. Apart from the parameters mentioned above, custom control for minimum surface size is made finer and coarsened according to different parts' geometric dimension.

Base size	50 mm
Target surface size	100%
Minimum surface size	8%
Surface growth rate	1.3
Volume growth rate	Slow
Maximum cell size	1600
Number of prism layers in interfaces	1
Number of prism layers in ground	400
Prism layer thickness in Ground	8

Table 3.8: Mesh setting for parts facing ambient fluid

The parts in the ambient fluids are meshed using trimmed cell mesh. A volumetric refinement box is created around the area that is closer to the vehicle in order to capture the physical phenomenon happening around the area of interest accurately.
Each part's prism layers are refined and thickened according to the requirement stated in the wall treatment section. General guidelines to be followed is to have minimum surface sizes of contact prevention, surface wrapper, and surface remesher in the ratio of 4:2:1, respectively. This is to avoid surface wrapper, capturing extremely finer areas that are difficult for executing mesh operation.

3.5 Simulation setup

3.5.1 Moving reference frame

The rotating objects in a steady-state simulation used can be modeled with a stationery mesh by means of moving the reference frame. The fan in the cooling system is modeled by this approach. The fan used in the simulation has inlet and outlet interfaces. The boundary condition is provided in such a way that the interfaces rotate along with fan blades. It is essential to specify the fan shroud as a stationary object.

3.5.2 Interfaces

Star-CCM+ interfaces are used to transfer quantities such as mass, momentum, and energy between different regions. In Star-CCM+, the internal interface is used to combine two different regions of the same continuum. Some of the interfaces conformal at the geometry level, whereas some interfaces do not need to coincide exactly. These interfaces need imprinting so that the common surface between two regions coincides exactly with each other. The imprinting feature in Star-CCM+ helps in achieving this. The interface quality can be checked by initializing the interface. In this simulation model, most of the internal interfaces have 99 percent conformable with each other.
In Star-CCM+, the heat exchanger interface is created between porous media of two different continua. To be specific, an external side and an internal are combined to form a heat exchanger interface. Creating this heat exchanger interface enables us to specify 'Q map,' which eventually paves the way to control the behavior dual-stream heat exchangers. The 'Q map' contains a table for cold and hot mass flows and their respective heat rejection values. The 'Q map' interpolates and calculates the power of heat exchanger(Q) values for the specific mass flow value rates.

3.5.3 Porous coefficients

Explicitly meshing very minute geometries such as air filters, bug net is computationally costly and tedious to perform. Thus an alternative way is to use the porous coefficients. The porous coefficients pose a resistance for the quantities passing through it. There are two types of porous coefficients, namely viscous and inertial resistance.

$$\frac{\Delta p}{L} = -(P_i|v_s| + P_v)v_s \tag{3.1}$$

Where P_i and P_v are inertial and viscous coefficients.v_s is the superficial velocity . The values of Δp , L , v_s are known from the test from which the P_i and P_v are calculated.

3.5.4 Physics continuum

Fluid	Depending on the continua
Wall Treatment	Two layer all y+
Energy model	Segregated fluid temperature
Solver type	Segregated flow
Gradients method	Hybrid Gauss-LSQ
Gravity	only for ambinet fluid
Turbulence model	Realizable K-Epsilon two layer
Time	Steady

Table 3.9: Star-CCM+ models used in the simulation.

Ambient air, CAC air, radiator coolant, Oil coolant are assigned to four different continua. Models for each continuum are chosen according to the physics to be simulated. The table above specifies the models used in the simulation. The initial conditions and reference values are specified here, and they influence the convergence of the solution.

Fluid

The continua models for all four continua are the same except the type of fluid used. The ambient fluid continua should be provided with ideal gas with constant density. The CAC continua model uses ideal gas with varying density. The radiator coolant continua use H2O as fluid. Note that during the test done by suppliers, the radiator was tested with water as the coolant. In the real-life scenario, the radiator coolant is a blend of glycol and H2O. The Oil cooler continua use H2O as fluid instead of oil.

Solver

The segregate flow solver is used in the simulation. The segregate flow solver's feature is that it solves the continuity, momentum one after another, whereas, in a coupled solver, they are solved in parallel. The SIMPLE algorithm is used for pressure velocity coupling. Second-order Upwind scheme is the numerical scheme used for the discretizing process. Algebraic Multigrid linear solver, commonly known as AMG linear solver, is the iterative solvers used to solve the discretized equations.

Gradients

The numerical scheme makes the variable values to be available at the cell center and cell faces. Likewise, the 'Gradients' allows values such as pressure gradient, secondary gradients, and velocity gradients to be available at the cell center and cell faces. The calculation of gradients involves using the following two-step algorithm. The calculation of unrestricted gradients uses the Hybrid Gauss-Least Square method. The unrestricted gradients refer to values that are not bounded by neighboring cells. The next step is limiting the unrestricted gradients to incorporate the scalar values at the faces.

Segregated fluid temperature

The energy model preferred for this simulation is segregated fluid temperature. The energy equation is solved with temperature as unknown. After finding the temperature, the enthalpy is later computed with the help of the equation of state. The second-order upwind scheme is used for the discretizing process. For this model, segregated fluid temperature is suitable for simulations without the involvement of combustion.

3.5.5 Boundary conditions

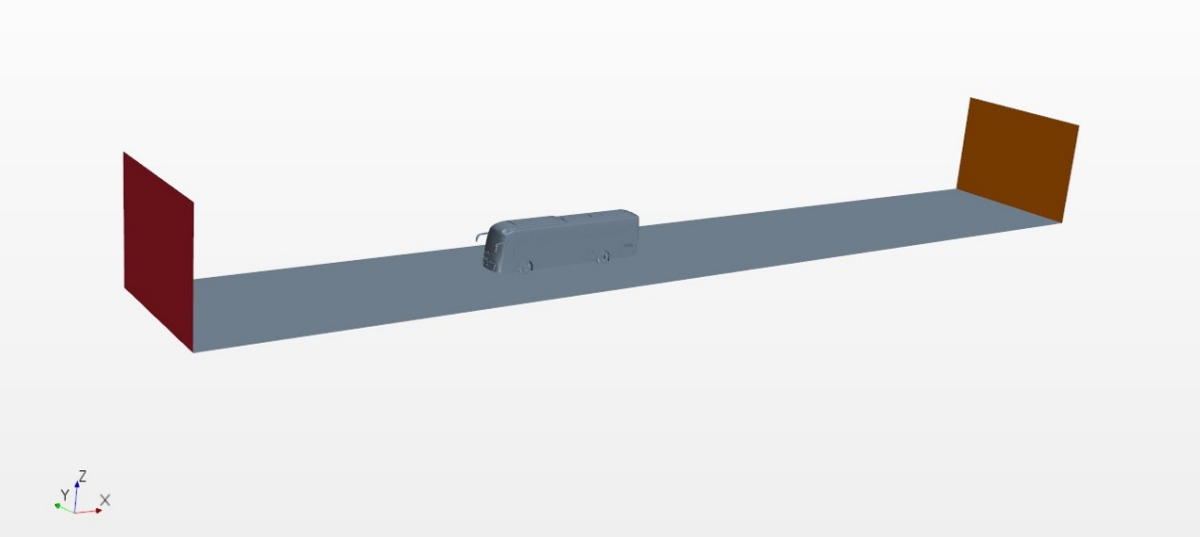

Figure 3.11: Domain setup

The simulation model is tested in four different cases. All four cases have different ambient air conditions and fan duty cycles, according to which other parameters are tuned. The test data sheet provides an exact boundary condition to be prescribed for various parts. As shown above, the domain has a velocity inlet for the

ambient air to enter and pressure outlet. It is made sure that the domain inlet, outlet, side planes are placed sufficiently far from the geometry. The sides of the domain are symmetric planes. The ground has a tangential velocity component equal to the inlet velocity of the ambient air. This is implemented to avoid boundary layers between ground and vehicle. The tires are provided with tangential velocities as,

$$V_{tangential} = \frac{speed}{r_{tyre}} \tag{3.2}$$

$V_{tangential}$ refers to tangential velocity, r_{tyre} refers to tyre radius and speed here refers to vehicle speed.
Since the radiation is not modeled, some of the underhood components are provided with surface temperature to make the simulation much more realistic. This temperature is based on experience. The inlet of the pipes are mass flow inlets, and outlets are pressure outlets. The mass flows are slowly ramp up to the maximum values through linearly interpolated table values. This is done to ensure solver convergence. The external side has inlets and outlets for ambient air. Likewise, the internal side has inlets and outlets for the coolant side. The other parts in the respective cores are walls. The heat exchanger pipes do not form a closed loop meaning that it does not represent the real-time conditions in which the pipes are connected to the engine. An equation is formulated to close the loop for fluids passing through heat exchangers and engine in the simulation model, This allows us to specify the coolant temperature based on heat rejection values and thereby complete the loop without the pipes representing the actual geometry. This simplification reduces the computational efforts. Since radiation is not modeled in the simulation model, the temperature in solid components is specified as surface temperature. In terms of accuracy, this is not a good practice.

4 Results

The results from four different cases of the underhood simulation model is presented below. The only difference between all four cases is the boundary conditions. The solver setting, mesh, continua models and the simulation setup is exactly the same. The contours and graphs for all the parameters depicted below are normalized for the Volvo bus's confidentiality purpose. The GT-SUITE simulation model and testing process are not a part of this thesis work. The data from GT-SUITE and test results are only used for making comparisons and evaluate the Star-CCM+ simulation model.

4.1 Heat Exchangers

This section mainly focuses on three main quantities associated with the heat exchangers.

- power of heat exchanger
- temperature
- pressure drop

A discussion between GT-SUITE, Star-CCM+ and test results are also presented below.

4.1.1 CAC

The boundary conditions associated with CAC for all four cases are listed below.

Cases	$\dot{m}_{External,CAC}$	$\dot{m}_{Internal,CAC}$	$T^{In}_{Internal,CAC}$	$P^{In}_{Internal,CAC}$
1	0.9	0.085	5.86	13.43
2	0.68	0.082	6.25	15.086
3	0.68	0.073	6.06	15.58
4	0.32	0.048	5.13	13.68

Table 4.1: CAC boundary conditions

where '$\dot{m}_{External,CAC}$', '$\dot{m}_{Internal,CAC}$', '$T^{In}_{Internal,CAC}$', '$P^{In}_{Internal,CAC}$' refers to CAC external side mass flow, CAC internal side mass flow, CAC internal side inlet temperature and CAC internal side inlet pressure respectively. The '$\dot{m}_{External,CAC}$' depends on the fan speed. The '$\dot{m}_{Internal,CAC}$', '$T^{In}_{Internal,CAC}$', '$P^{In}_{Internal,CAC}$' are boundary conditions with which the test were conducted.

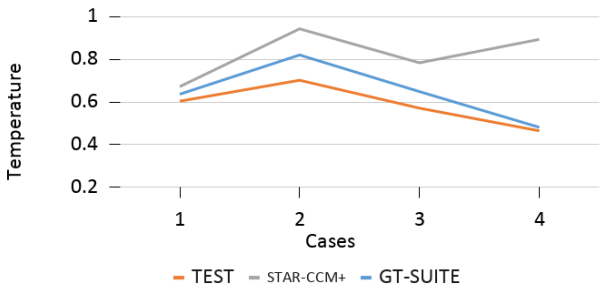

Figure 4.1: Mass flow averaged CAC internal side outlet temperature ($T^{Out}_{Internal,CAC}$)

CAC internal side outlet temperature ($T^{Out}_{Internal,CAC}$) difference between four cases is shown in fig 4.1. The CAC coolant usually has a huge temperature difference between inlet and outlet because CAC's internal fluid is air, which is the same as external fluid. The mass flow averaged temperatures are calculated at CAC's internal outlet interface and compared with GT-SUITE and test results. Accuracy of the $T^{Out}_{Internal,CAC}$ heavily relies on the type and parameters of oil used in oil coolers. The fact that this simulation model does not replicate the type and temperature of oil used during the test may influence the simulation results' deviation.

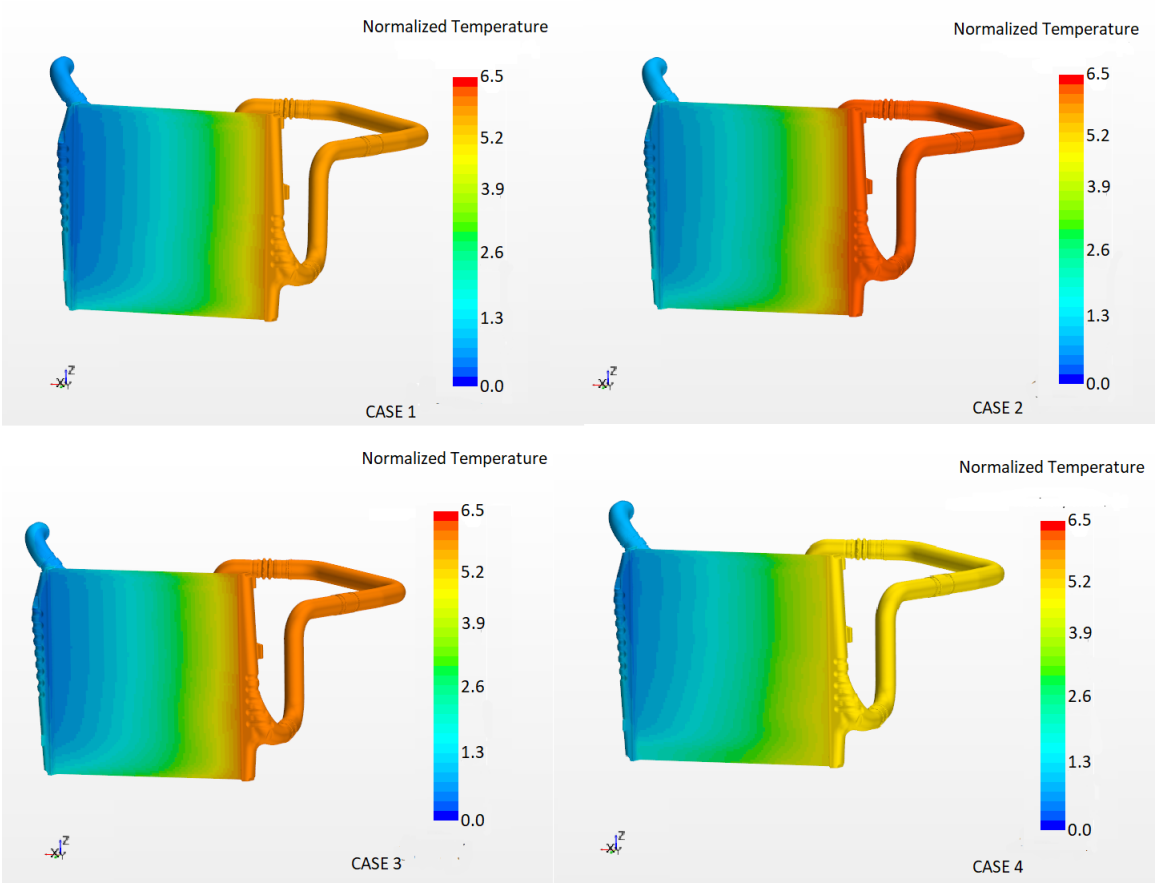

Figure 4.2: CAC internal side temperature-cut section

A cut section through the center of the CAC internal side is made and the temperature is depicted above for all 4 cases in fig 4.2. The hot coolant enters from the right side and interacts with the ambient air traveling perpendicular to it and cools down due to conduction and convection as it flows towards the outlet on the left side.

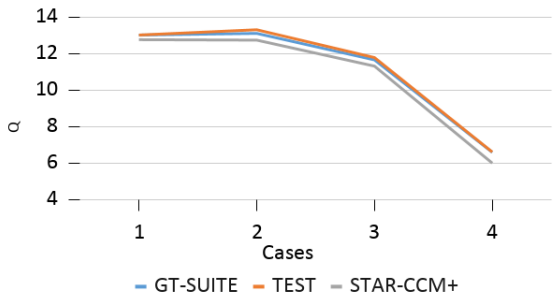

Figure 4.3: Power of CAC heat exchanger (Q_{CAC})

The 'Q map' from test data specifies a heat exchanger's power (Q) in the simulation model. So it common to have a good agreement in Q between the test and simulation model. Though the CAC has lower power than the radiator, the difference in temperature is higher between the inlet and outlet of the internal side($\Delta T_{internal,CAC}$). The reason behind this is the internal side fluid used for CAC (charge air) has a lower specific heat capacity than the internal side fluid used for the radiator(water).

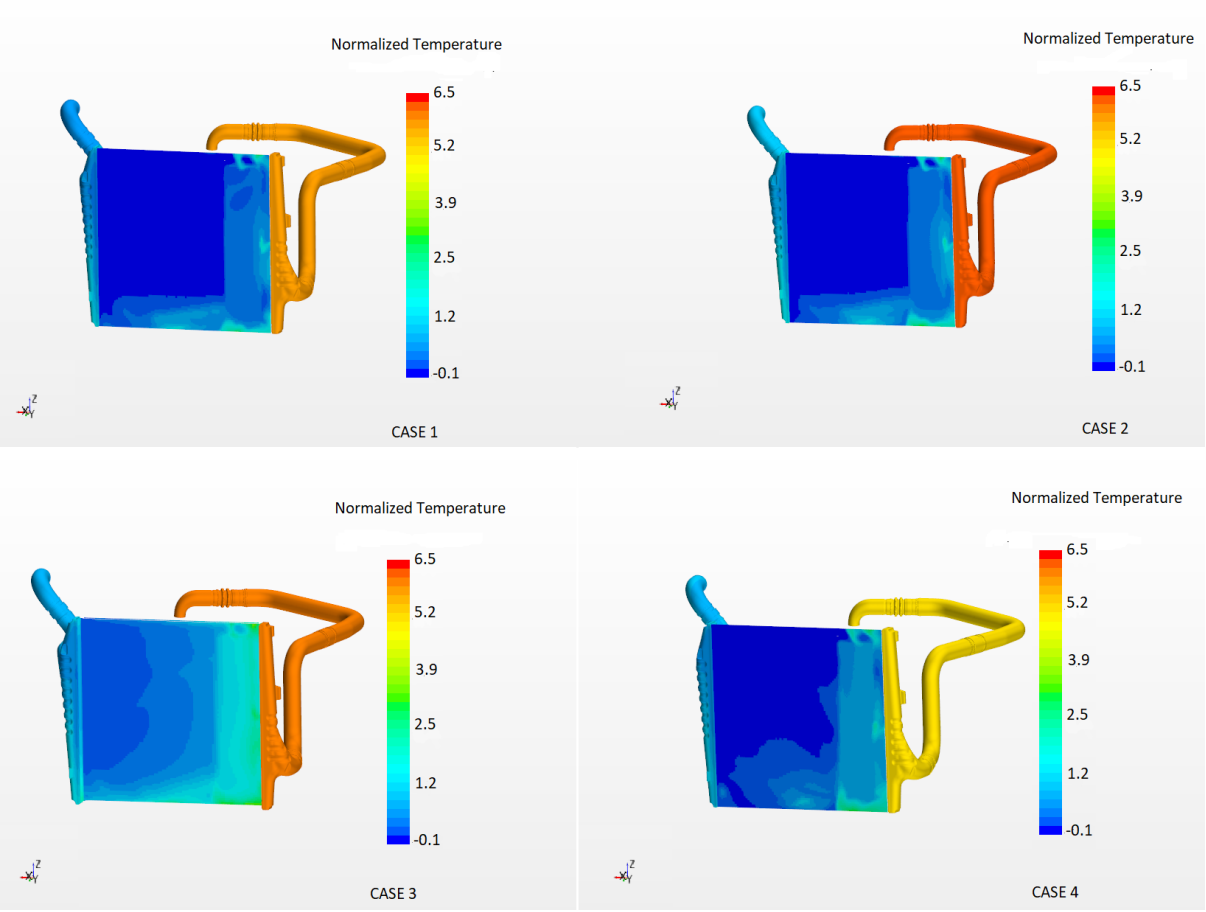

Figure 4.4: CAC external side inlet temperature ($T^{In}_{External,CAC}$)

The CAC external side inlet temperature $T^{In}_{Internal,CAC}$ is shown in fig 4.4. The oil cooler external side outlet imprints higher temperatures on a particular portion of CAC's external side's inlet due to sandwich. The remaining part of the CAC is directly exposed to ambient air. Fig 4.4 shows a specific region (right side and bottom) of CAC has higher temperatures than other areas. The CAC external side outlet is an area through which the ambient air escapes after cooling down the charge air. The ambient air before escaping attains higher temperatures and flows into radiator external side inlet. This hot ambient air tends to heat other components in the underhood.

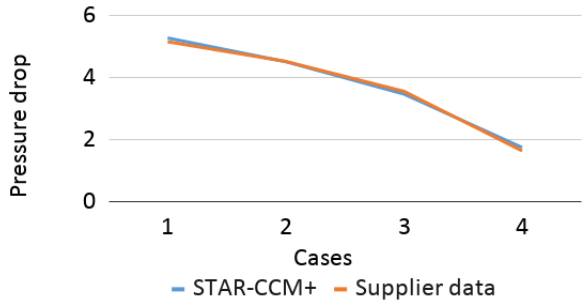

Figure 4.5: CAC internal side pressure drop $\Delta P_{Internal,CAC}$

A reliable simulation depends on how psychical the assumptions are made to match reality. In this simulation, actual porous media with tiny holes are substituted with porous coefficients values. It is essential to make sure that these values agree well with the simulation results. One way of doing that is to compare the pressure

drop values of internal and external sides between simulation and test data for the mass flows with which they are carried out. The difference in pressure drives the flow from an inlet to an outlet. The CAC internal side pressure drop ($\Delta P_{Internal,CAC}$) values are presented above in fig 4.5. Suppliers have tested the heat exchangers for a range of mass flows and found the respective pressure drop values. The $\Delta P_{Internal,CAC}$ values from the simulation results have a good match up with the supplier tested $\Delta P_{Internal,CAC}$ values (fig 4.5).

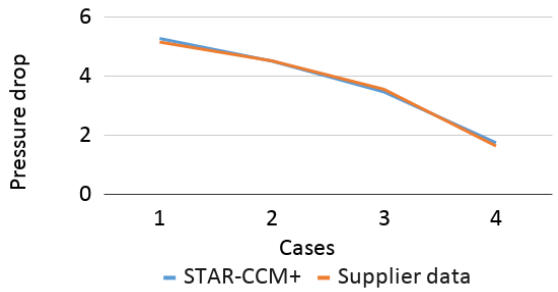

Figure 4.6: CAC external side pressure drop $\Delta P_{External,CAC}$

The variations of pressure drop values for CAC external side ($\Delta P_{External,CAC}$) concerning all four cases are depicted above in fig 4.6. A higher mass flow rate induces a higher pressure drop, which explains why case 1 has a higher $\Delta P_{External,CAC}$. The $\Delta P_{External,CAC}$ depends on the mass flow generated by fan speed. It is essential to cross-check the values with supplier specified values. By doing so, the correctness in the simulation setup can be made sure. The $\Delta P_{External,CAC}$ in the simulation have an excellent agreement with the supplier values as it should be.

4.1.2 Radiator

The table below summarizes the boundary condition used for the radiator.

Cases	$\dot{m}^{In}_{External,RAD}$	$\dot{m}^{In}_{Internal,RAD}$
1	0.94	0.085
2	0.71	0.082
3	0.68	0.073
4	0.35	0.048

Table 4.2: Radiator boundary conditions

where '$\dot{m}^{In}_{External,RAD}$', '$\dot{m}^{In}_{Internal,RAD}$', refers to mass flow at radiator external side inlet and mass flow at radiator internal side inlet respectively. It is worth mentioning that these mass flow values are not from experimental data.

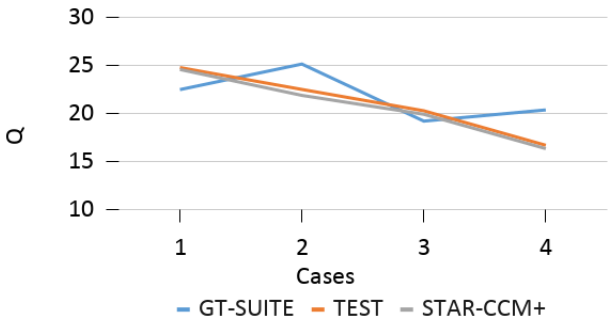

Figure 4.7: Power radiator heat exchanger (Q_{RAD})

The hot coolant entering of the radiator is cooled down by ambient air. Unlike CAC which follows gas-gas interaction, the liquid-gas interaction occurs in the radiator to achieve the desired cooling. Recall the fact that the coolant being used is water. The specific heat capacity (cp) of water is 4.18 $\frac{KJ}{KgK}$, which is much higher than the air with a cp of 1.008$\frac{KJ}{KgK}$. This statement says that to change the water temperature by 1-degree Celsius, 4.18 KJ of energy needs to be supplied. Observing the graphs, it can be seen that the Q_{RAD} is higher, and temperature difference between ($\Delta T_{Internal,RAD}$) is lower when compared to CAC. The deviations in GT-SUITE values are may be due to calibration error with test data.

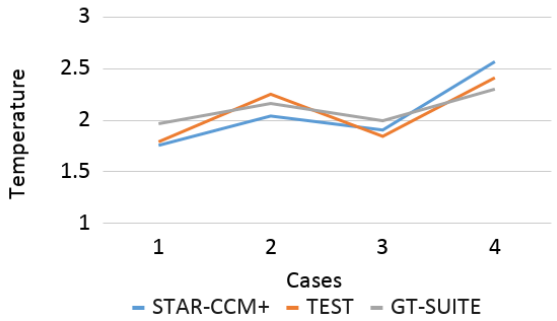

Figure 4.8: Mass flow averaged radiator internal side inlet temperature ($T^{In}_{Internal,RAD}$)

The internal side inlet temperature ($T^{In}_{Internal,RAD}$) is one of the crucial parameters that need to be verified. The boundary condition section describes the closed-loop formulation and why the radiator needs it. Formulated loop in the form of equation needs validation and is presented in fig 4.8. Radiator internal side inlet mass flow ($\dot{m}^{In}_{Internal,RAD}$) values from testing could give a better agreement between the simulation model and test data in fig 4.8.

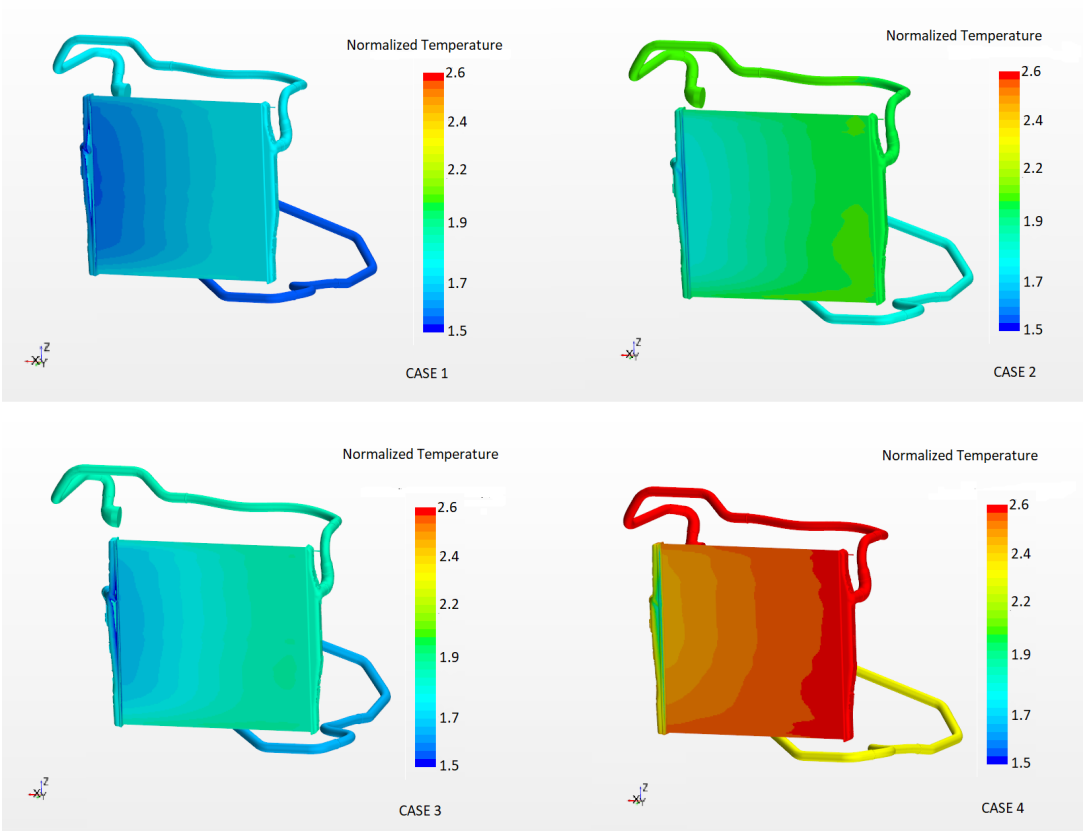

Figure 4.9: Radiator internal side temperature- cut section

A cut section through the centerline of internal side of the radiator is shown in fig 4.9. Case 4 has the highest coolant temperature. The boundary conditions for case 4 it is known that the vehicle is operated at a low fan fan duty cycle, ultimately leading to a lower cooling system's fan RPM. Fan operating at lower RPM pulls in inadequate mass flow of ambient air, which is the primary agent responsible for cooling the internal side's fluid. All these factors lower the Q_{RAD} as seen in fig 4.7, and thereby the coolant in case 4 has a higher internal side outlet temperature ($T^{out}_{Internal,RAD}$), which in turn because of the reflects the higher ($T^{In}_{Internal,RAD}$).

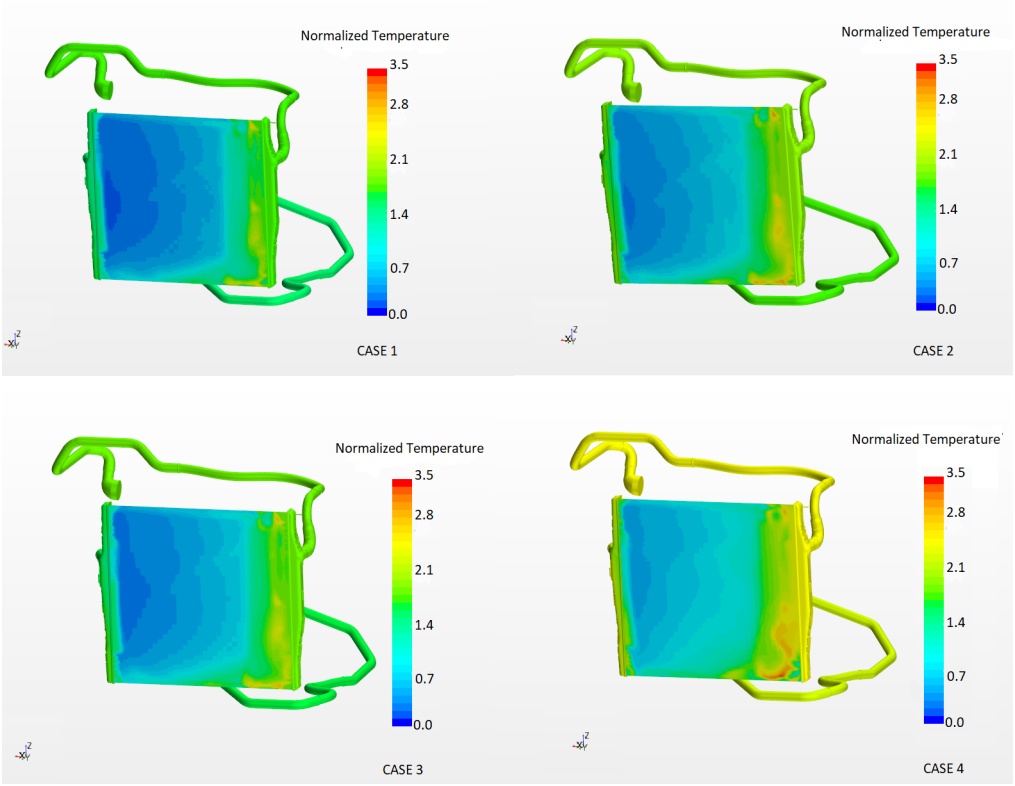

Figure 4.10: Radiator external side inlet temperature ($T^{In}_{External}$: RAD)

The external side inlet temperature of the radiator ($T^{In}_{External,RAD}$) is higher compared to CAC and oil cooler. The radiator is the last heat exchanger in the sandwich arrangement. The radiator is followed by a fan spinning at high velocity. The ambient air passing through the oil cooler and CAC attains an increase in temperature and imprints them in the radiator. The ambient air leaving the radiator passes through the fan, heating underhood components before its exit from the underhood trough the provisions provided. Some of these ambient air is also recirculated back to the heat exchanger.

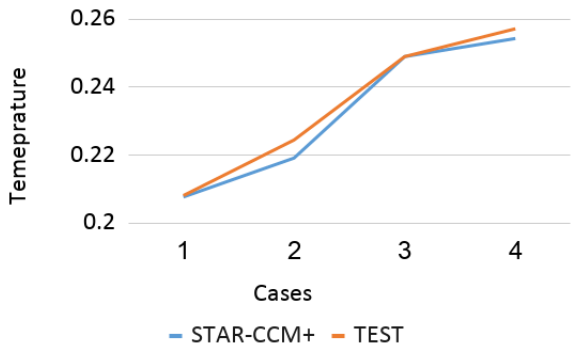

Figure 4.11: Mass flow averaged internal side temperature difference ($\Delta T_{Internal,RAD}$)

Q_{RAD} is responsible for this excellent correlation between experimental and simulation values of $\Delta T_{Interna,RAD}$ in fig 4.11. With a very good agreement between test and simulation values of Q_{RAD} and ($\Delta T_{Internal,RAD}$), it further strengthens the argument under fig 4.9 about the specification of accurate ($\dot{m}^{In}_{Internal,RAD}$) values for closing the loop.

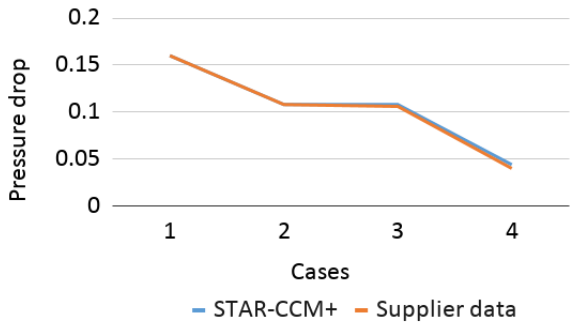

Figure 4.12: Radiator external side pressure drop ($\Delta P_{External,RAD}$)

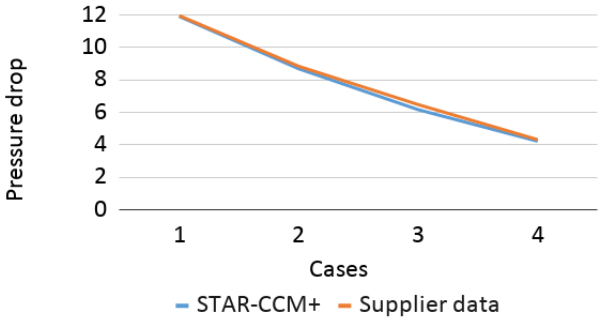

Figure 4.13: Radiator internal side pressure drop ($\Delta P_{Internal,RAD}$)

The pressure drop values for external and internal side for the radiator are shown above in fig 4.12 and fig 4.13. The pressure drop values are identical comparing Star-CCM+ and supplier's data, which eventually justifies the values of the porous coefficients provided at the radiator's internal and external interfaces in the simulation setup.

4.1.3 Oil cooler

The oil cooler is the first heat exchanger facing the ambient fluid. The geometry and orientation of the oil cooler are different from CAC and radiator. As mentioned earlier, there are no test data available for the oil cooler. The boundary conditions that are based on experience and practice are listed below.

- Cp_{oil}
- Q_{oil}
- $\dot{m}_{Internal,Oil}$
- $T^{In}_{Internal,Oil}$

where, 'Cp_{oil}', 'Q_{oil}', '$\dot{m}_{Internal,Oil}$', '$T^{In}_{Internal,Oil}$' are specific heat capacity of oil, power of oil cooler, oil cooler internal side mass flow inlet, oil internal side inlet temperature respectively.
In this simulation 'property-changed' H2O is used as fluid substitute for the hydraulic oil. The Cp value used is 2.5 $\frac{KJ}{KgK}$ which is a good approximation for hydraulic oil. The type of hydraulic oil used is an unknown and so dynamic viscosity, density and thermal conductivity values are approximated based on properties of commonly

available oil . The Q_{oil} and $T_{In}^{Internal} : Oil$ is based on experience. The only accurate value for oil cooler that mimics the test conditions is $\dot{m}_{external} : Oil$, since it is based on fan speed.

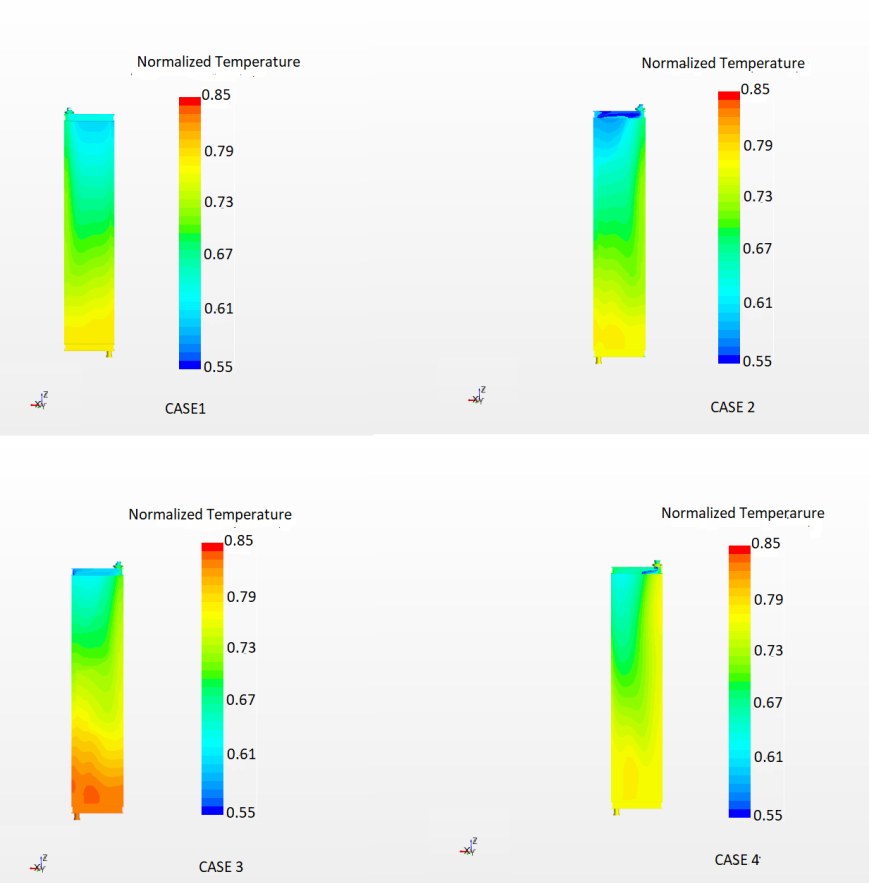

Figure 4.14: Oil internal side temperature-cut section

The oil cooler internal side cut section is depicted in fig 4.14. The hot fluid enters on the lower side and exits through the upper side of heat exchanger. The fluid flow is against the buoyancy which usually causes unstable stratification. The phenomenon unstable stratification causes rise in temperature. In this cases the heat transfer is governed by forced convection which neutralizes the unstable stratification effect.

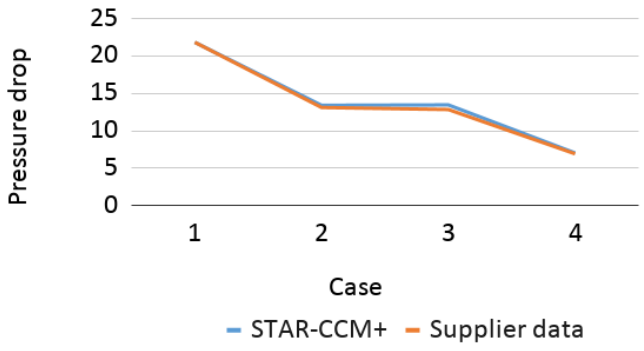

Figure 4.15: Oil internal side pressure drop ($\Delta P_{Internal,Oil}$)

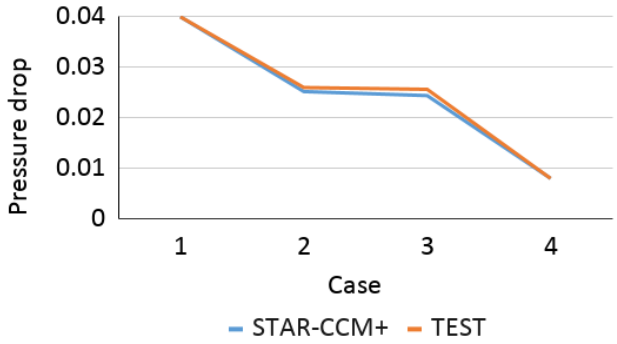

Figure 4.16: Oil external side pressure drop ($\Delta P_{External,Oil}$)

The pressure drop for oil cooler's internal side ($\Delta P_{Internal,Oil}$) and external side ($\Delta P_{External,Oil}$) is presented above and evaluated against supplier data. As it is seen the porous coefficients calculated have no issues since the pressure drop have a good agreement with the test results.

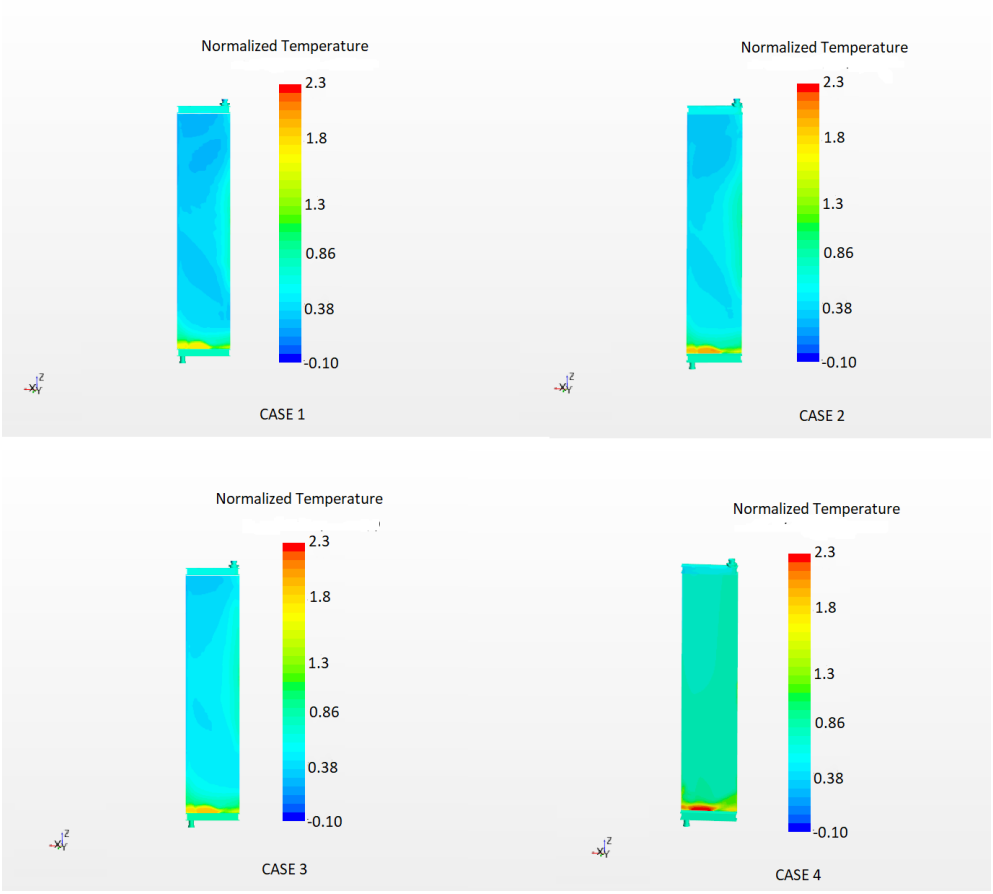

Figure 4.17: Oil external side outlet temperature ($T_{Out}^{External} : Oil$)

The oil cooler external side outlet temperature $T_{External,Oil}^{Out}$ is shown in the fig 4.17. $T_{External,Oil}^{Out}$ is imprinted on CAC heat exchanger since it is closest to oil cooler. The case 4 have highest $T_{External,Oil}^{Out}$ which explains the reason for highest temperature in case 4 of the $T_{Internal,CAC}^{In}$.

4.2 Performance

The estimation of the parameters presented in this section helps engineers predict the operating point of the vehicle. A summary of LAT and IMTD is as follows. The LAT is calculated to determine the maximum ambient air temperature at which a vehicle can be operated. IMTD is used to find the difference in air temperatures coming from two sources, at the inlet manifold of the combustion chamber. Currently, recirculation is an unavoidable feature and estimating it judges the overall design of the vehicle.

4.2.1 LAT and IMTD

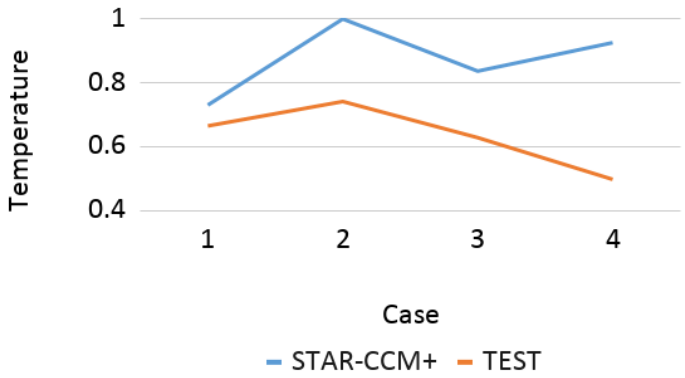

Figure 4.18: Inlet manifold temperature difference (IMTD)

The inlet manifold temperature difference (IMTD) is compared between test and simulation for all four cases. From the comparisons, the IMTD in Star-CCM+ deviates from test results. Arguably this may be due to the reason mentioned above concerning oil cooler parameters.

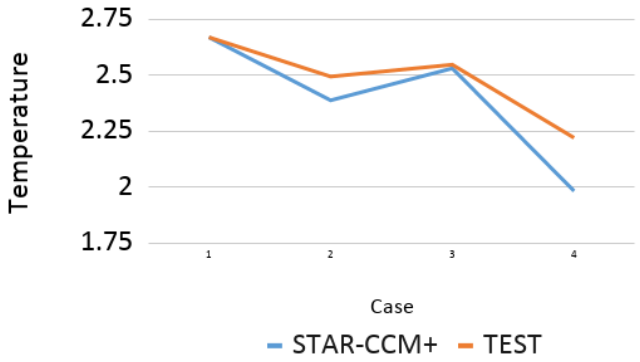

Figure 4.19: Limiting ambient temperature (LAT)

The limiting ambient temperature (LAT) is compared between Star-CCM+ and test results. The limiting ambient air temperature for case 1 and case 3 have a good agreement. Case 2 and Case 4 have vsisble variation. Revisiting the formula to find LAT, one can see the usage of $T^{In}_{Internal,RAD}$. As already mentioned in the discussion under fig 4.8, the comparison in fig 4.19 can be drastically improved with the massflow values.

4.2.2 Recirculation

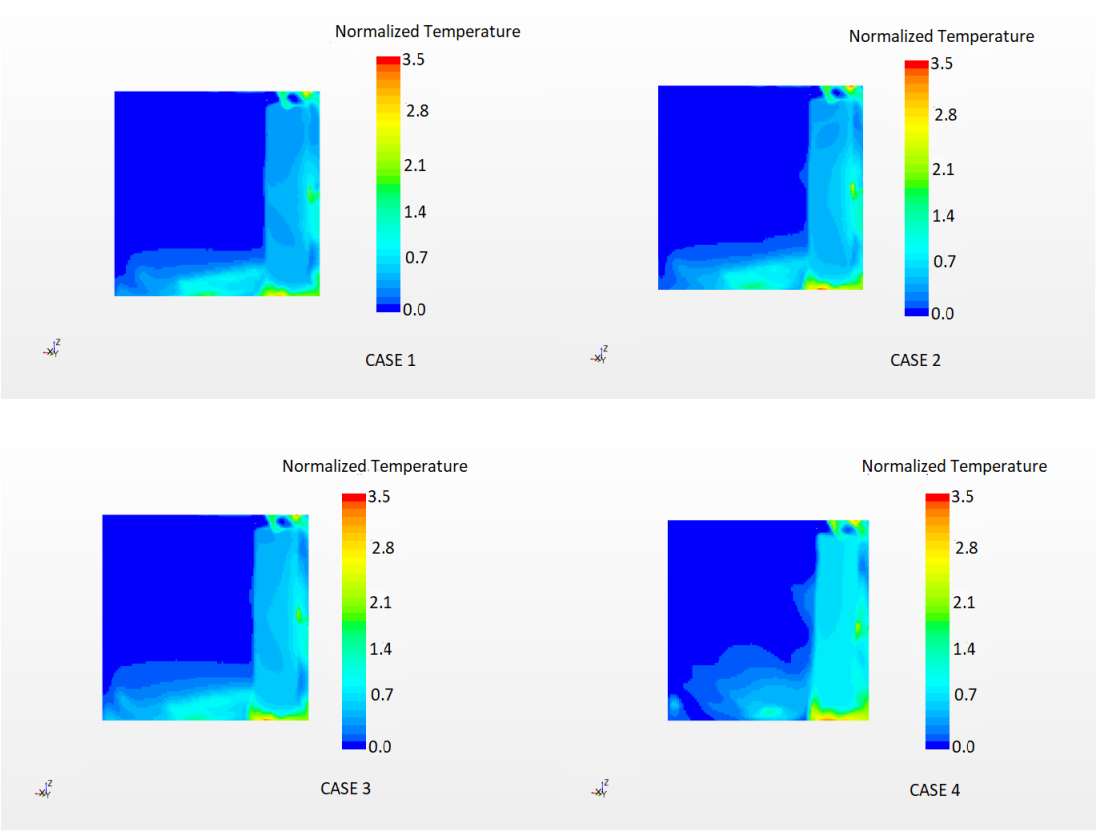

Figure 4.20: Recirculation temperature ($T_{recirculation}$)

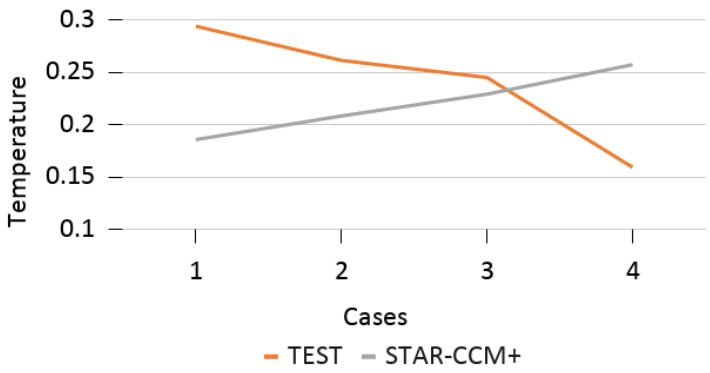

Figure 4.21: Mass flow averaged recirculation temperature $T_{recirculation}$

The recirculation temperature ($T_{recirculation}$) occurring at CAC external side inlet is shown in fig 4.20 and the results are compared with the test data in fig 4.21. The $T_{recirculation}$ trend predicted by star-CCM+ is not aligned with the test results. Prediction of $T_{recirculation}$ requires an immense amount of accuracy in replicating the actual physics. Without modeling radiation, it is hard to get a reliable $T_{recirculation}$ from the model. Once again, the parameters for oil coolers also impact the $T_{recirculation}$ prediction in the model.

0,0	0,0	0,0	0,0	0,0	0,0	0,0	0,0	0,0	0,2	0,3
0,0	0,0	0,0	0,0	0,0	0,0	0,0	0,0	0,0	0,3	0,2
0,1	0,1	0,1	0,1	0,2	0,1	0,1	0,1	0,1	0,4	0,1
0,3	0,4	0,5	0,5	0,6	0,6	0,6	0,6	0,7	0,6	0,5

Figure 4.22: $T_{recirculation}$ from test

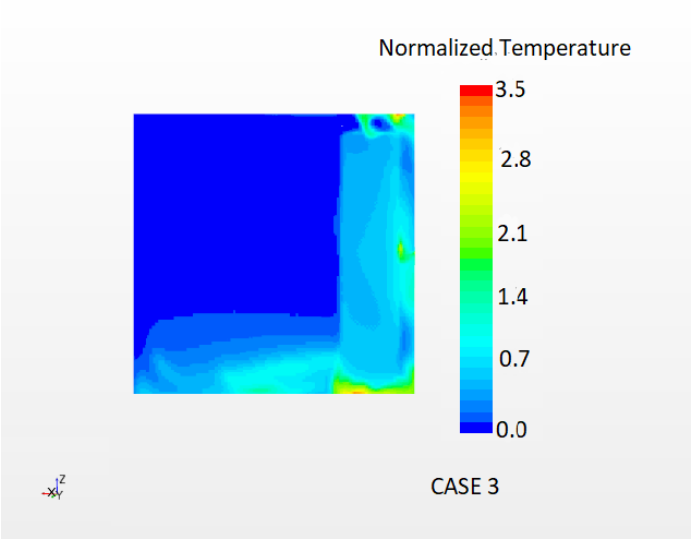

Figure 4.23: $T_{recirculation}$ from Star-CCM+

The fig 4.22 at top shows section-wise $T_{recirculation}$ temperature from test for case 3. The red color borders indicate the sensor failure in those sections. The fig 4.23 bottom indicates the $T_{recirculation}$ from Star-CCM+ for the same case. The high-temperature region at the bottom and right are right behind the oil cooler.

4.3 Underhood Temperature

This section presents the underhood floor temperature of the simulation model of all four cases. The radiation is not modeled in the simulation. The temperature variations are only due to boundary condition variation between all four cases. As it is clearly seen in the case, 4 shows higher temperatures, which is purely due to boundary conditions. The fan speed in case 4 is very low, which explains the concentration of temperature in a confined region around the engine compartment.

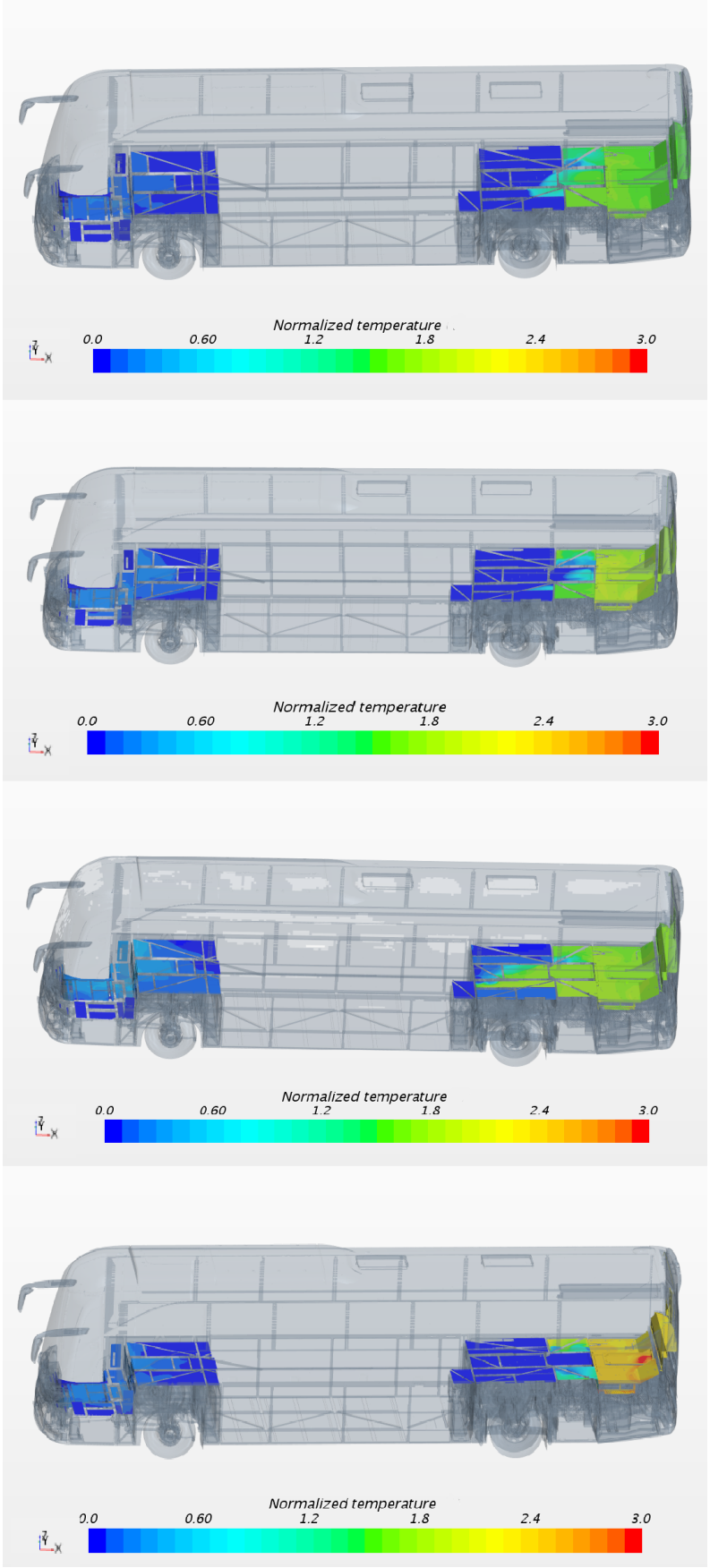

Figure 4.24: Bus floor temperature

5 Conclusion and Future Scope

The overall objective of the thesis table is to develop a 3D simulation model that combines cooling system performance with the whole underhood simulation model is achieved. Another essential goal satisfied in the angenda is to replace the practice of modeling heat exchangers as single stream type with dual stream type. Four different test cases are considered for simulation. All the relevant comparisons between the test results, Star-CCM+ results, GT-suite results are made. Discussions about deviation in a few comparisons are also elaborated. Talking about the comparisons, one of the things to keep in mind is that GT-SUITE simulations are calibrated against the test results.

There are a few things that will surely increase the reliability of the model. First and foremost, the data for oil coolers from real-time testing is required and extremely important to get the desired results. Other than all the data being available, some more significant contributions may come from modeling radiation. Modeling radiation requires heat transfer coefficient data for different materials present in the underhood of the vehicle. The last thing to consider is the topology of test tracks and accounting for side winds.

Overall, this simulation model will be a perfect starting point in terms of getting the model working, which can get tricky with the implementation of dual stream heat exchanger model. Accounting for the above said suggestions would be future scope for this project. This would very well allow VBC to have greater control over performance aspects before the production stage.

References

[Bah+18] R. Bahuguna et al. "Design and Development of Cooling System for a Formula SAE Race Car". *SAE Technical Paper*. SAE International, Apr. 2018. DOI: 10.4271/2018-01-0079. URL: https://doi.org/10.4271/2018-01-0079.

[BW09] M. Balhoff and M. Wheeler. A Predictive Pore-Scale Model for Non-Darcy Flow in Porous Media. *SPE Journal* **14** (Nov. 2009), 579–587. DOI: 10.2118/110838-MS. URL: https://doi.org/10.2118/110838-MS.

[Çen03] Y. A. Çengel. *Heat transfer : a practical approach.* McGraw-Hill series in mechanical engineering. McGraw-Hill, 2003. ISBN: 0072458933. URL: https://search.ebscohost.com/login.aspx?direct=true&AuthType=sso&db=cat07470a&AN=clc.a153dbac.5e08.4f1f.8ea9.c312647be22a&site=eds-live&scope=site&custid=s3911979&authtype=sso&group=main&profile=eds.

[Dav15] L. Davidson. *Fluid mechanics, turbulent flow and turbulence modeling*. 2015.

[Laa05] C. Laaksometsä. *CFD study of the heat transfer modes in engine cooling systems.* [Examensarbete] (Deparment of Energy and Environment): [2005:6]. Chalmers tekniska högskola, 2005. URL: https://search.ebscohost.com/login.aspx?direct=true&AuthType=sso&db=cat07470a&AN=clc.a0b59f15.29aa.4426.8d68.8f83928ac959&site=eds-live&scope=site&custid=s3911979&authtype=sso&group=main&profile=eds.

[Red13] J. N. Reddy. *An Introduction to Continuum Mechanics*. 2nd ed. Cambridge University Press, 2013. DOI: 10.1017/CBO9781139178952.

[ROD] W. RODI. "Experience with two-layer models combining the k-epsilon model with a one-equation model near the wall". *29th Aerospace Sciences Meeting*. DOI: 10.2514/6.1991-216. eprint: https://arc.aiaa.org/doi/pdf/10.2514/6.1991-216. URL: https://arc.aiaa.org/doi/abs/10.2514/6.1991-216.

[Shi+95] T.-H. Shih et al. A new k- eddy viscosity model for high reynolds number turbulent flows. *Computers Fluids* **24**.3 (1995), 227–238. ISSN: 0045-7930. DOI: https://doi.org/10.1016/0045-7930(94)00032-T. URL: http://www.sciencedirect.com/science/article/pii/004579309400032T.

[VM07] H. Versteeg and W. Malalasekera. *An Introduction to Computational Fluid Dynamics: The Finite Volume Method*. Pearson Education Limited, 2007. ISBN: 9780131274983. URL: https://books.google.se/books?id=RvBZ-UMpGzIC.

[WXG05] A. Wang, Z. Xiao, and H. Ghazialam. "Evaluation of the Multiple Reference Frame (MRF) Model in a Truck Fan Simulation". *Vehicle Thermal Management Systems Conference Exposition*. SAE International, May 2005. DOI: https://doi.org/10.4271/2005-01-2067. URL: https://doi.org/10.4271/2005-01-2067.